การพิมพ์สามมิติของวัสดุเชิงประกอบแกรฟีน/เทอร์โมพลาสติกอิลาสโตเมอร์

นายวรยุทธ คณะเบญจ

วิทยานิพนธ์นี้เป็นส่วนหนึ่งของการศึกษาตามหลักสูตรปริญญาวิทยาศาสตรมหาบัณฑิต
สาขาวิชาวิทยาศาสตร์พอลิเมอร์ประยุกต์และเทคโนโลยีสิ่งทอ ภาควิชาวัสดุศาสตร์
คณะวิทยาศาสตร์ จุฬาลงกรณ์มหาวิทยาลัย
ปีการศึกษา 2560

3D PRINTING OF GRAPHENE/THERMOPLASTIC ELASTOMER COMPOSITES

Mr. Warrayut Kanabenja

A Thesis Submitted in Partial Fulfillment of the Requirements
for the Degree of Master of Science Program in Applied Polymer Science and Textile Technology
Department of Materials Science
Faculty of Science
Chulalongkorn University
Academic Year 2017

Thesis Title	3D PRINTING OF GRAPHENE/THERMOPLASTIC ELASTOMER COMPOSITES
By	Mr. Warrayut Kanabenja
Field of Study	Applied Polymer Science and Textile Technology
Thesis Advisor	Associate Professor Pranut Potiyaraj, Ph.D.

Accepted by the Faculty of Science, Chulalongkorn University in Partial Fulfillment of the Requirements for the Master's Degree

.....Dean of the Faculty of Science

(Professor Polkit Sangvanich, Ph.D.)

THESIS COMMITTEE

.....Chairman

(Associate Professor Duangdao Aht-Ong, Ph.D.)

.....Thesis Advisor

(Associate Professor Pranut Potiyaraj, Ph.D.)

.....Examiner

(Associate Professor Kawee Srikulkit, Ph.D.)

.....External Examiner

(Supachoak Tanpichai, Ph.D.)

วรยุทธ คณะเบญจ : การพิมพ์สามมิติของวัสดุเชิงประกอบแกรฟีน/เทอร์โมพลาสติกอิลาสโตเมอร์ (3D PRINTING OF GRAPHENE/THERMOPLASTIC ELASTOMER COMPOSITES) อ.ที่ปรึกษาวิทยานิพนธ์หลัก: รศ. ดร. ประณัฐ โพธิยะราช, 81 หน้า.

เส้นวัสดุเชิงประกอบเทอร์โมพลาสติกพอลิยูรีเทนกับแกรฟีนถูกเตรียมขึ้นโดยกระบวนผสมแบบหลอมเหลวด้วยเครื่องอัดรีดสกรูคู่ก่อนนำไปใช้งานร่วมกับเครื่องพิมพ์สามมิติเพื่อขึ้นรูปเป็นชิ้นงาน จากนั้นศึกษาผลของปริมาณแกรฟีนที่ใส่ลงในพอลิเมอร์ตั้งแต่ร้อยละ0.05 ถึง 0.20 โดยน้ำหนัก ต่อสมบัติของวัสดุเชิงประกอบ ขั้นแรกเป็นขั้นตอนสังเคราะห์แกรไฟต์ออกไซด์จากแกรไฟต์ผ่านกระบวนการออกซิเดชันด้วยวิธีของฮัมเมอร์ตามด้วยขั้นตอนของการเปลี่ยนโครงสร้างของแกรฟีนออกไซด์ให้กลายเป็นแกรฟีนผ่านกระบวนการรีดักชันด้วยกรดแอลแอสคอร์บิก ซึ่งยืนยันจากเทคนิคฟูเรียร์ทรานสฟอร์มอินฟราเรดสเปกโทรสโกปีและการวิเคราะห์การเลี้ยวเบนรังสีเอกซ์ นำชิ้นงานเทอร์โมพลาสติกพอลิยูรีเทนและวัสดุเชิงประกอบระหว่างเทอร์โมพลาสติกพอลิยูรีเทนกับแกรฟีนมาวิเคราะห์สมบัติ ได้แก่ สมบัติทางความร้อน สมบัติเชิงกล สมบัติทางกายภาพ และสมบัติทางไฟฟ้า ผลการทดลองพบว่าวัสดุเชิงประกอบมีเสถียรภาพทางความร้อนที่ดีขึ้นเมื่อเปรียบเทียบกับเทอร์โมพลาสติกพอลิยูรีเทน โดยเมื่อพิจารณาวัสดุเชิงประกอบในสูตรที่มีการเติมแกรฟีนร้อยละ 0.15 โดยน้ำหนัก พบว่าวัสดุเชิงประกอบมีการสลายตัวทางความร้อนขั้นแรกและขั้นที่สองสูงขึ้นจากเดิมถึง 3 และ 4 องศาเซลเซียสตามลำดับ นอกจากนี้ยังพบว่าการเติมแกรฟีนยังส่งผลต่ออุณหภูมิการหลอมเหลวของพอลิเมอร์ให้มีค่าที่สูงขึ้นด้วย เมื่อวิเคราะห์ด้วยเครื่องวัดมุมสัมผัสพบว่าการเพิ่มปริมาณแกรฟีนยังส่งผลต่อสมบัติความไม่ชอบน้ำของตัวพอลิเมอร์ให้มากขึ้นอีกด้วย ในกรณีของสมบัติเชิงกลพบว่าวัสดุเชิงประกอบในสูตรที่มีปริมาณแกรฟีนร้อยละ 0.05 โดยน้ำหนัก มีความทนแรงดึงและเสถียรภาพทางรูปร่างที่สูงที่สุดเมื่อเปรียบเทียบกับวัสดุเชิงประกอบในสูตรอื่น

ภาควิชา วัสดุศาสตร์ ลายมือชื่อนิสิต .....

สาขาวิชา วิทยาศาสตร์พอลิเมอร์ประยุกต์และเทคโนโลยีสิ่งทอ ลายมือชื่อ อ.ที่ปรึกษาหลัก .....

ปีการศึกษา 2560

5972050423 : MAJOR APPLIED POLYMER SCIENCE AND TEXTILE TECHNOLOGY
KEYWORDS: GRAPHENE / THERMOPLASTIC POLYURETHANE / COMPOSITES / 3D PRINTING / FUSED DEPOSITION MODELING

WARRAYUT KANABENJA: 3D PRINTING OF GRAPHENE/THERMOPLASTIC ELASTOMER COMPOSITES. ADVISOR: ASSOC. PROF. PRANUT POTIYARAJ, Ph.D., 81 pp.

Graphene based thermoplastic polyurethane composites filaments was prepared by melt blending process prior to fabricate with 3D printing technique. The effects of different graphene loading (0.05 wt% - 0.20 wt%) in TPU matrix on the properties of composites were studied. Initially, graphite was successfully oxidized to graphite oxide following Hummer's method and the reduction of graphene oxide to graphene by L-ascorbic acid was also achieved as being confirmed by the FTIR and XRD results. TPU and TPU/graphene nanocomposites were investigated for their thermal, mechanical, physical and electrical properties. Thermal stability of TPU/graphene composites was improved against neat TPU. The first and second degradations of 0.15 wt% filled nanocomposites increased about 3 °C and 4 °C. The thermal properties of nanocomposites were studied by DSC and the result show the higher melting temperature when compared with neat TPU. The hydrophobicity of nanocomposites increased with the higher loading of graphene in TPU as observed by the contact angle measurement. The nanocomposites with 0.05wt% of graphene addition showed the highest tensile strength and dimensional stability.

Department:	Materials Science	Student's Signature	.....
Field of Study:	Applied Polymer Science and Textile Technology	Advisor's Signature	.....
Academic Year:	2017		

ACKNOWLEDGEMENTS

This thesis successfully accomplishes the expected objectives due to the invaluable encouragement from many benefactors. The propitious suggestions and collaborations bring me on the right and appropriated decision during the thesis composition. Thereby, I would like to express my sincere thanks to all supporters.

1. My advisor, Associate Professor Pranut Potiyaraj, Ph. D., his great motivation, inspiration, helpful suggestion, good attitude, high patience throughout the thesis course are significant participants of my work. All parts of my thesis are revised by him to improve the completeness of my thesis. Moreover, I would like to thank him for his financial support, laboratory space and research methodology for my research.

2. Prasit Pattananuwat, Ph. D., and Chuanchom Aumnate, Ph.D. who give research instructions and helpful advices in the laboratory.

3. Thesis committees, the beneficial academic suggestion during the thesis defense presentation.

4. Center of Excellence in Petrochemicals and Materials Technology, Chulalongkorn University, the financial support through the experiment.

5. Department of Materials Science, Faculty of Science, Chulalongkorn University, the supporter of characterization instruments, experimental machine and area.

6. Vinyltec industry, the thermoplastic polyurethane materials (Elastollan S85A) supporter for this thesis.

7. Mr. Aphiwat Pongwisuthiruchte, he advise and collaborate with all of my thesis.

8. Miss Nichaphat Passornraprasit, her comment on my work give me a wider aspects.

9. Kittinon Sakunphokesup, finding a suitable condition for 3D printing fabrication.

Finally, I would like to thank my family about the motivations and supports throughout my whole life.

CONTENTS

Page

THAI ABSTRACT iv

ENGLISH ABSTRACT v

ACKNOWLEDGEMENTS vi

CONTENTS vii

Chapter 1 Introduction 1

1.1 background and problem 1

1.2 Objectives 2

Chapter 2 Literature review 3

2.1 3D printing 3

2.1.1 Timeline of 3D printing 3

2.1.2 Types of 3D printing 4

2.1.3 3D printing software 7

2.2 Thermoplastic elastomer 8

2.3 Thermoplastic polyurethane 8

2.3.1 Synthesis of thermoplastic polyurethane 9

2.4 Graphene 11

2.4.1 Graphene production 11

2.4.2 Properties of graphene 15

2.5 Composites 16

2.5.1 Types of composite 17

2.5.2 Polymer/graphene nanocomposite 17

Chapter 3 Experiment 19

Page

3.1 Materials and chemicals 19
3.2 Processing machine 19
3.3 Characterization instruments and testing machines 20
3.4 Experimental flow chart 21
3.5 Experimental procedure 22
3.5.1 Graphene preparation 22
3.5.1.1 Synthesis of graphite oxide 22
3.5.1.2 Conversion of graphite oxide to graphene 22
3.5.2 composite filament preparation 23
3.5.2.1 Masterbatch preparation 23
3.5.2.2 Composite filaments preparation 23
3.5.3 3D printing fabrication 24
3.5.3.1 program design 24
3.5.3.2 Specimen printing 24
3.6 Characterization and testing 26
3.6.1 X-ray diffractometry, XRD 26
3.6.2 Fourier transform infrared spectrometry, FT-IR 26
3.6.3 Differential scanning calorimetry, DSC 27
3.6.4 Thermogravimetric analysis, TGA 28
3.6.5 Melt flow index, MDI 28
3.6.6 Shore A hardness test 29
3.6.7 Contact angle 29
3.6.8 Tensile test 30

Page

3.6.9 Scanning electron microscopy....30
Chapter 4 Results and discussions....32
4.1 Characterization of graphite, graphite oxide and graphene....32
4.1.1 X-ray diffractometry....32
4.1.2 Fourier transform infrared spectroscopy....33
4.2 Materials characterization....34
4.2.1 Differential scanning calorimetry....34
4.2.2 Thermal gravimetric analysis....36
4.2.3 Melt flow index....37
4.2.4 Hardness....38
4.2.5 Contact angle....38
4.2.6 Tensile properties....39
4.2.7 Scanning electron microscopy....41
Chapter 5 Conclusions and suggestions....44
5.1 Conclusions....44
5.2 Suggestions....45
REFERENCES....46
APPENDIX....52
Appendix a Fourier transform infrared spectroscopy, FTIR....53
Appendix b Differential scanning calorimetry, DSC....55
Appendix c Thermal gravimetric analysis, TGA....59
Appendix d Melt flow index....61
Appendix e Hardness....63

Page

Appendix f Contact angle.....65

Appendix g Tensile properties 67

Appendix h Electrical conductivity.....77

VITA.....81

List of figures

Chapter 2

Figure 2.1 hard segment and soft segment phase separation 9

Figure 2.2 polyester based thermoplastic polyurethane synthesis 10

Figure 2.3 polyether based thermoplastic polyurethane synthesis 10

Figure 2.4 Allotropes of carbon [15] 11

Chapter 3

Figure 3.1 Experimental flowchart 21

Figure 3.2 Twin screw extruder model Prism DSR-28 24

Figure 3.3 in-house wind-up machine 24

Figure 3.4 3D printer model Wanhao Duplicator 6 25

Figure 3.5 X-ray diffractometer (Bruker AXS D8 Advance X-ray diffractometer) 26

Figure 3.6 Fourier transform infrared spectrometer (Thermo Scientific model Nicolet 6700) 27

Figure 3.7 Differential scanning calorimeter (Mettler Toledo, DSC 1 STAR System) 27

Figure 3.8 Thermogravimetric analyzer (Mettler Toledo, TGA/DSC 3^{+} STAR System) 28

Figure 3.9 Melt flow indexer (model 7053) 28

Figure 3.10 Hardness durometer Shore A (Shore) 29

Figure 3.11 Contact angle meter (model CAM-PLUS) 29

Figure 3.12 Universal testing machine (model H10KM) 30

Figure 3.13 Scanning electron microscope (JEOL JSM-6480LV) 30

Figure 3.14 High resistance meter (Agilent model 4339B) 31

Chapter 4

Figure 4.1 X-ray diffractrogram of a) graphite, b) graphite oxide, c) graphene.....33

Figure 4.2 FTIR spectra of a) graphite, b) graphite oxide, c) graphene. 34

Figure 4.3 DSC thermograms of a) TPU and nanocomposites with b) 0.05, c) 0.10, d) 0.15 and e) 0.20 wt% of graphene at cooling step. 35

Figure 4.4 DSC thermograms of a) TPU and nanocomposites with b) 0.05, c) 0.10, d) 0.15 and e) 0.20 wt% of graphene at second heating step.....35

Figure 4.5 TGA thermogram of TPU and nanocomposites. 37

Figure 4.6 Melt flow index of TPU and nanocomposites.....37

Figure 4.7 Hardness of TPU and nanocomposites. 38

Figure 4.8 Contact angle of TPU and nanocomposites. 39

Figure 4.9 Stress at 100 mm extension of TPU and nanocomposites.....40

Figure 4.10 Young's modulus of TPU and nanocomposites. 40

Figure 4.11 Unbroken TPU/0.05G specimens 41

Figure 4.12 Surface morphology image of a),f) TPU, b),g) TPU/0.05G, c),h) TPU/0.10G, d),i) TPU/0.15G and e),j) TPU/0.20G at 1,500 and 5,000 magnification respectively.....42

Figure 4.13 Resistance of TPU and nanocomposites. 43

Figure 4.14 Conductivity (σ) equation 43

Figure 4.15 Electrical conductivity of TPU and nanocomposites. 43

List of tables

Chapter 3

Table 3.1 Controlled variables for 3D printing 25

Chapter 4

Table 4.1 Melting temperature of TPU and nanocomposites. 36

Table 4.2 Thermal properties of TPU and nanocomposites by TGA**.**.....36

Chapter 1

Introduction

1.1 background and problem

3D printing fabrication has been used widespread at this moment. 3D printing overcome the limitation of conventional processing techniques, i.e. injection molding or compression molding, due to its capability for complex product designing with the high quality of final products. Among various types of 3D printing techniques, a fused deposition modeling (FDM) is the most convenient and well-known because printing materials are easy to acquire and specific knowledge is not required for operation. The materials used for this 3D printing technique include several kinds of thermoplastic polymers in the commercial grade such as poly (lactic acid) (PLA), poly (vinyl alcohol) (PVA), acrylonitrile-butadiene-styrene (ABS), poly (ethylene terephthalate) (PET), thermoplastic elastomer (TPE), high impact polystyrene (HIPS), to name but a few. Each polymer has different pros and cons according to their characteristics. However, for each different grade polymer, a capability for using with 3D printing machines is also different such as PLA for injection molding is not suitable for use with the 3D process.

Thermoplastic polyurethane (TPU) which is one type of TPE based on urethane linkages is prevalently used worldwide. TPU is a multi-purpose synthetic polymer that has become substitution of the previous generation like thermoset rubber because of their advantages such as flexibility, easy processability, and reusability. Therefore, many thermoplastic elastomer-based products are used for common and specific applications like housewares, medical appliance, electronics tools, engineering tools, and automotive parts. TPU can be easily fabricated into the final products by injection molding or cast film extrusion. However, 3D printing of TPU is somewhat difficult due to its properties. Drop or string of TPU may occur during 3D printing leading to discontinue printing and unfilled product. To produce the effectively printable materials, some properties of TPU must be improved. In addition, researchers also aim to produce filament materials with additional properties, for example antistatic and high performance mechanical properties for value added in the industrial sector. There are several means to improve the properties of polymers. One of the popular solutions

is using the reinforcing agent. However, the amount and size of the reinforcing agent are the significant factors that need to be considered because the appropriate percentage of additive in polymers matrix is required to optimize the properties of the final product. The size of additive must be small enough to pass through the 3D printer's die or nozzle. Thus, graphene is selected for combining with thermoplastic elastomer because of its nano-scale sizes and excellent properties.

Graphene has become a disruptive technology because of the incredible properties such as lightweight, flexible, transparent, excellent strength and electrical conductibility. Since graphene has been found, Scientists from the whole world have been interested in it and find the way to use. Many researchers involved graphene by using its miraculous traits for improving the existing materials or to develop the new materials to open up the novel industry and marketing like graphene production and graphene-based product.

The aim of this research is to alter some properties of TPU of injection molding grade for suitable using with the 3D printer. Composites filaments between TPU and graphene were prepared by melt blending using a twin-screw extruder. The dispersion of graphene in TPU is a serious problem that needs to also be solved. To increase its dispersion, graphene was co-precipitated with TPU to prepare a masterbatch and then pre-mixed with pure TPU pellet prior to melt blending in twin-screw extruder. TPU and TPU/graphene filament were extruded in order to use with the 3D printer.

Graphite, graphene oxide, and graphene were characterized by X-ray diffraction spectroscopy (XRD) and Fourier transform infrared spectroscopy (FTIR).

TPU and composites filament were investigated by differential scanning calorimetry (DSC), thermogravimetric analysis (TGA), scanning electron microscopy (SEM), contact angle analysis, hardness (shore A) test, tensile tests.

1.2 Objectives

1. To tune the properties of TPU in order to make a suitable 3D printing filaments.
2. To evaluate the effect of graphene on antistatic properties and mechanical properties of thermoplastic polyurethane composites using 3D printing fabrication.

Chapter 2

Literature review

2.1 3D printing

2.1.1 Timeline of 3D printing

Although 3D printing has been worldwide accessed for recent last few decades, there was first prototype of 3D printing machine was created around 30 years ago. The first stereolithography (SLA) 3D printer was invented in 1983 by Chuck Hull which potentially printed the solid objects using the liquid UV curable material and UV light. Then, Hull founded his company names “3D Systems” and consider about his previous work that not only liquid can be used but any materials with efficiency of solidification or altering its physical state. So, 3D printing has been known as additive manufacturing (AM) from then [1].

New kinds of additive manufacturing has been continually released after the Hull’ patent titled “Apparatus for Production of Three-Dimentional Objects by Stereolithography” has been announced.

In 1987 at University of Texas, Carl Deckard created and patented new method called “selective laser sintering, SLS” that use laser sintering on loose powders to bind them together instead of curing monomer. The first SLS machine is named “Betsy”. Moreover, Larry Hornbeck creates “digital light processing” technology in same year.

In 1989, the co-founder of Stratasys, Scott Crump filed a patent for fused deposition modeling or FDM. After this patent has expired, there are many the desktop 3D printer companies declare their products to the world. However, many companies call “fused filament fabrication, FFF” instead of “FDM” because “FDM” is trademarked by Stratasys.

In 1992, 3D Systems creates the first SLA printer which is capable to fabricate complicated parts from layer by layer. In the same year, DTM produced the first SLS printer which use a laser sintering. Moreover, Stratasys announces the first commercial FDM printer “3D Modeler”.

In 1993, binder jetting was developed at Massachusetts Institute of Technology and licensed to Z Corporation on 1995. In 1994, Solidscape develops wax jetting.

In 2005, Dr. Adrian Bowyler found Rap Rap project at the University of Bath in England. This project seek for creating a low cost self-replicating manufacturing machine that can make most of its components and this is a beginning of 3D printing desktop for household usage.

In 2006, Objet debuts multiple material printing. So, SLS printer becomes commercially viable for mass customization which is the breakthrough the demand of industrial manufacturing. On 2007, 3D Systems releases first product with priced under $10,000.

2.1.2 Types of 3D printing

From the past few years, the evolution of 3D printing has been continuously developed while the price of 3D printers has decreased but their performance has been improved. Today, the desire of producing complicated design with high resolutions, reducing defects on products, rapid fabricating and enhancing mechanical properties is the main objective [2].

Totally, there are seven methods of 3D printing process.

1. Material extrusion: fused deposition modeling or FDM is the most flexible and common method which a solid thermoplastic filament is fed through by roller or motor and molten to semi-liquid state at heated nozzle. The printing move in X and Y direction on the platform while molten polymer deposit on a build plate and then the extrude cools and solidifies. After a first layer is completely printed, the nozzle is calculably moved up on Z direction and continuously print to the subsequent layer on the previous layer. The viscoelasticity of polymer is a significant property for this method which allows the polymer to melt during printing and then to set on the platform [2, 3]. There are many important factors such as layer thickness, width, orientation, air gap between each of printed parts and diameter of nozzle are the main parameters that affect the mechanical properties of

final products. Therefore, poor depositing, the unfulfilled layers and inferior surface quality are drawbacks of FDM [4]. However, cheap, fast fabrication time and simple process are main advantages of FDM [2].

2. Vat polymerization: there are two types of 3D printing including stereolithography (SLA) and direct light processing (DLP). For SLA, main substances for this technique are curable monomer solution and ultraviolet laser beam. To selectively cure and harden the polymer surface, mirror or galvanometers is used for instantaneous aiming the direction of laser on the X and Y axis. The laser beam moves on the cross-sectional area from point to point. The object is built up layer by layer from stacking the cross-sectional solidified layers [5]. The unreacted monomer is removed after printing and some printed part may be heated or photolytic cured after printed to improve the mechanical properties [2]. For DLP, all concepts is same with SLA but the difference is that DLP uses a digital light projector to flash a single image of entire layer at once. Light-emitting diode (LED) or Ultraviolet light source is directly radiate to the surface of resin by digital micromirror device (DMD) to build the layer [6].

3. Powder bed fusion: selective laser sintering or SLS uses thermal energy source and very fine powders. A laser beam induce the powders in each layer to fuse and pack together. After the total cross-sectional area is completely scanned, the build platform will move down one layer according to program setting. The recoating blade will fulfill powders on previous scanned layer, and then the subsequent layers are repeatedly scanned on top of previous layers and fused together until the product is fully built [2]. Powder size distribution and packing which determine the density of final object are the most essential factors for this method [7]. Not only polymers can be used with SLS but metals and alloy powders can

be also used. This method is unnecessary to support the structures because the remaining powder which hasn't been sintered is still maintain the object [6].

4. Material jetting: material jetting (MJ) and drop on demand (DOD) are sub class of this method. For MJ, the inkjet head injects tiny UV curable polymer droplets and then instantly solidifies them using UV light on the substrate. The build plate will move down one step of height after one layer has already hardened and continually print next layers until the work is done. MJ is different from other types of additive manufacturing because materials is deposited, sintered or cured in one line but others is in one point. Multiple objects fabrication in a single line with no impact on print speed and fabrication speed are advantages of this technique. For DOD, there are 2 materials, first one is wax-like material and second one is dissolvable support material. Both of product and supporter are printed layer by layer until finish printing. The supporter and objects are dissolved in liquid solution to remove support material [6].

5. Binder jetting: the principle of binder jetting or BJ is similar to SLS that powder layer is prepared on the build platform but it use liquid binder droplets instead of laser beam to fuse powder together. Once a layer has done, the platform is lowered down and new powder layer is refilled over the previous layer. The chemistry and rheology of binder, size and shape of powder particles, deposition speed, the interaction between powder and binder are the crucial factors in this method [7, 8].

6. Laminated object manufacturing: laminated object manufacturing or LOM is one of commercial 3D printing. This method base on layer by layer by

mechanical or laser cutting and lamination of sheets or rolls of materials. Layers are accurately cut and then bonded together between layers.

7. Direct energy deposition: direct energy deposit or DED is a method used with metal. Metal powder or wire is instantly melted by laser or electron beam in order to deposit on the substrate and then metal is solidified after laser beam pass through.

2.1.3 3D printing software

Computer aided design or CAD is a computer technology for product design and process design documentation which replaces a manual drafting. CAD is helpful for 3D printing process by facility of transferring detailed diagrams of product's materials, processes variables, dimensions and tolerances. It can make either 2D or 3D diagrams with ability of rotation for looking from any angles even inside or outside that reduce the defect of final product. Many programs are suitable for the beginner but some of them is required for user's printing professional design to create more complicated objects. CAD can create STL file that is necessary for 3D printing manipulation.

A STL file stores information about 3D models. This format illustrates only the surface geometry of 3D object without any color, texture or other common model attributes. Cooperation of slicer with STL file allows a computer to communicate with 3D printer hardware. Slicer is a piece of 3D printing software that converts digital 3D models into printing instructions for 3D printing object. The slicer chops STL file into several pieces of flat horizontal layers based on the settings. The programs will calculate the amount of material and printing time for printing. All of this information is then bundled up into a GCode file that is the native language of 3D printer. Therefore, the quality of printed object is depended on an accuracy of slicer setting. Once the GCode has been uploaded to printer, the next step is reassembly of separated 2D layers into 3D object on build platform. The printing is done when object is successively deposited [9].

2.2 Thermoplastic elastomer

Thermoplastic elastomer or TPE is a very flexible thermoplastic polymer which completely regenerate itself into original dimension after stress releasing at room temperature. Now a day, TPEs are classified into 2 main types block copolymer and thermoplastic/elastomer blends & alloys. There are styrenics, copolyesters, polyurethanes and polyamides for block copolymer. There are thermoplastic polyolefins and thermoplastic vulcanizates for thermoplastic/elastomer blends & alloys. Typically, thermoplastic elastomer consists of 2 main phases including hard thermoplastic phase with high glass transition temperature and soft elastomer phase with low glass transition temperature. These 2 segments bind together by physical bonding or chemical bonding [10].

2.3 Thermoplastic polyurethane

Thermoplastic polyurethane or TPU is a one kind of thermoplastic elastomers that is chemically synthesized from diisocyanate, polyol and diol as chain extender to form urethane linkage [11]. TPU contains two structural phases due to the intrinsic incompatibility between the hard segments and soft segments. Urethane linkages are the hard segment and these segment are available to move near together and form hydrogen bonding between carbonyl and amino to form crystalline. The aggregation and orientation of hard segment form into hard domain that act as physical crosslinking which is similar to chemical crosslinking in vulcanizates. The hard domain behave as a dimensional regeneration or elasticity of TPU. For soft segments, they are divided to many types according to their chemical structure and functional group such as aliphatic hydrocarbon, polyester based and polyether based TPU. The existence of this aliphatic soft elastomer segment is a main reason for non-crystalline or amorphous region. So, TPU can be stretched and change its dimension because of the appearance of amorphous domain. The hard domains are below their glass transition temperature that is the main parts for hysteresis, permanent deformation, modulus and strength of material. The soft domains are above their glass transition temperature and exhibit the

property of rubber-like material at room temperature. Typically, the hard domains are immersed in a rubbery soft segment matrix but some are isolated in a soft domain determine by hard segment content as shown in Figure 2.1 [12]. However, the properties of polyurethanes depend on soft segment chemical structure, hard segment chemical structure, molecular weight of soft segment and hard segment and the proportion between the hard segment and the soft segment. Thus, their properties like abrasive resistance, heat resistance, low temperature flexibility, heat aging, hydrolysis resistance, chemical resistance, microbial resistance, adhesion strength, Injectability and mechanical properties are related to the type of polyol, diisocyanate and chain extender.

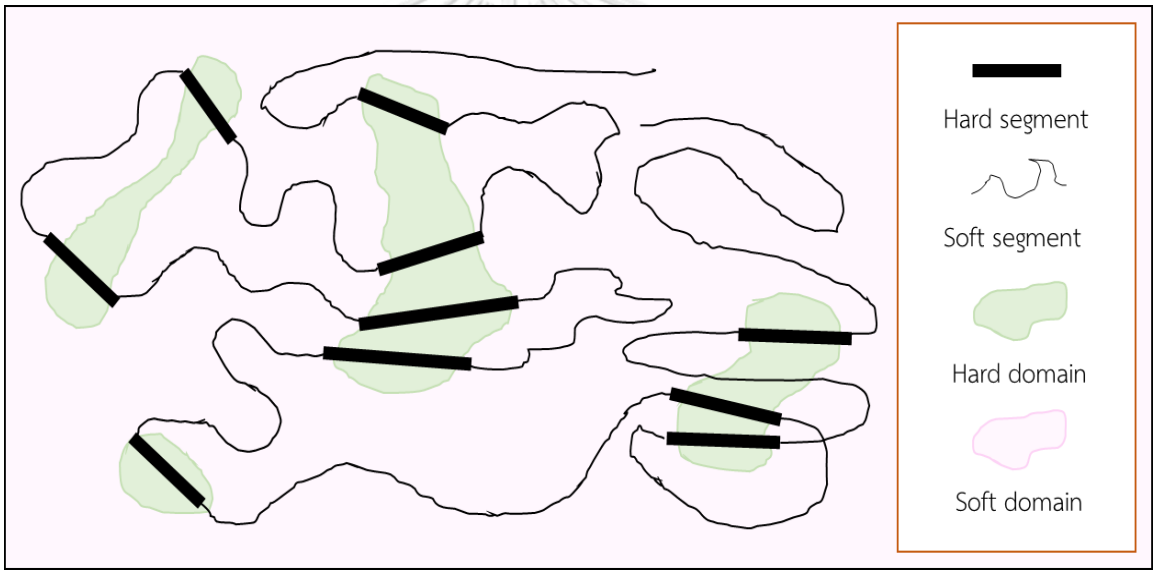

Figure 2.1 hard segment and soft segment phase separation

2.3.1 Synthesis of thermoplastic polyurethane

Normally, thermoplastic polyurethanes are synthesized via condensation polymerization between hydroxyl and isocyanate groups. There are many methods to synthesize TPU. Most of them use the same principle except their prepolymer. In a case of polyester based TPU, prepolymer is polymerized from dicarboxylic acid with excess diol or polyol prior to condense with excess diisocyanate to produce NCO terminated prepolymer. For polyether based TPU, polyether is obtained from ring opening polymerization prior to polymerize with diisocyanate to produce NCO

terminated prepolymer. Both of NCO terminated prepolymer is then condense with chain extender to extend its backbone as showed in Figure 2.2 and Figure 2.3.

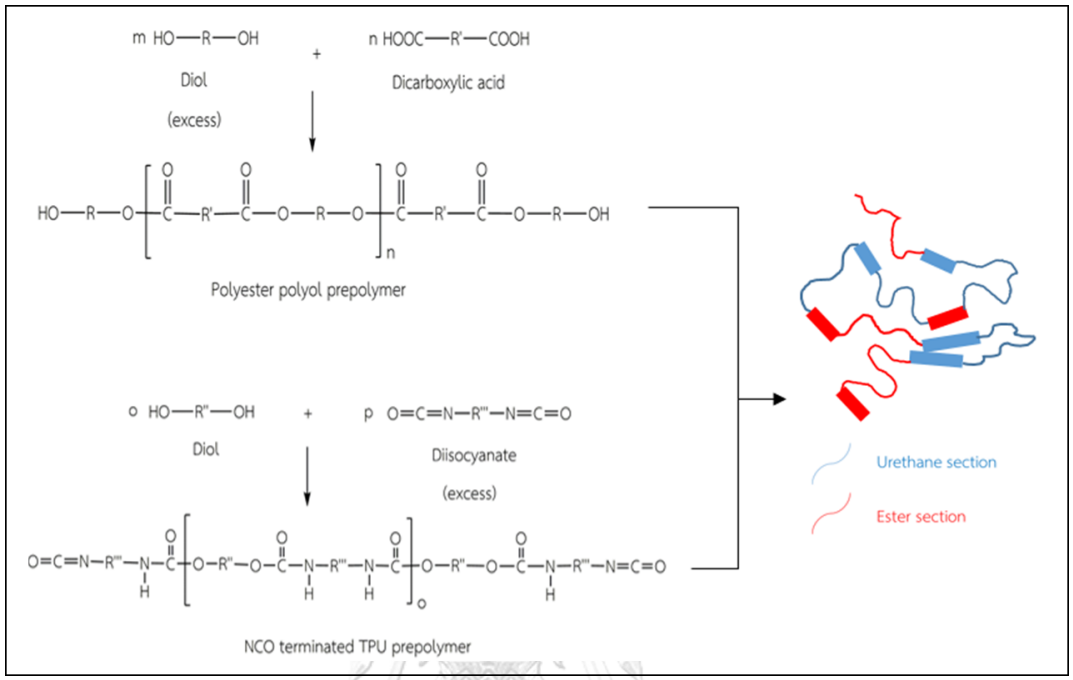

Figure 2.2 polyester based thermoplastic polyurethane synthesis

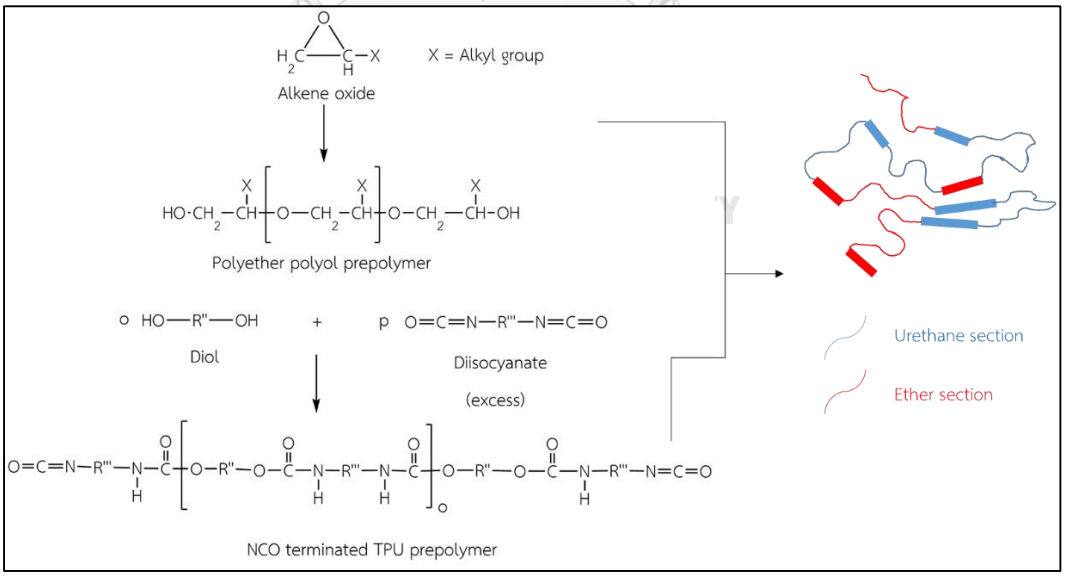

Figure 2.3 polyether based thermoplastic polyurethane synthesis

2.4 Graphene

On 2004, graphite was successfully exfoliated into graphene by two scientists, Prof. Andre Geim and Prof. Kostya Novozelov at University of Manchester, England. Graphene is a two dimensional single layer of pure carbon atom with sp^2 hybridization arranged in continuous hexagonal configuration. Graphene is a base of fullerenes, carbon nanotube and graphite as concluded in Figure 2.4. Scientists believe that two dimensional materials probably occur the decomposing or collapse into more stable carbon allotropes due to their thermodynamically unstable at finite temperature [13], but graphene is the first stable two dimensional materials that can freely occupy by itself because of the atomic scale ripples on the graphene's surface that minimize the surface energy [14].

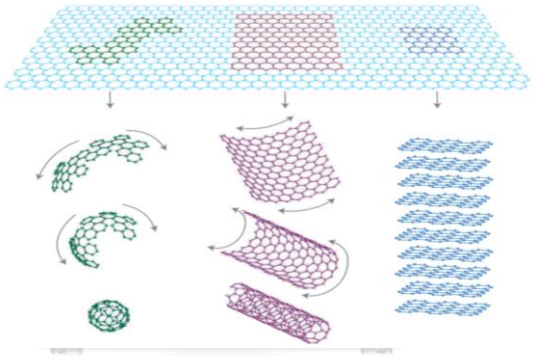

Figure 2.4 Allotropes of carbon [15]

2.4.1 Graphene production

After the first discovery, a fabrication method of graphene become an interesting method. The aim of graphene production is high quality of graphene with high production scale and low cost [16]. The new routes of graphene production has been develop to overcome this problem. There are many methods including micromechanical cleavage (MC), liquid phase exfoliation (LPE), chemical reduction of graphene oxide, bottom up synthesis, chemical vapor deposition (CVD) and electrochemical exfoliation are selected to access the graphene production.

1. Micromechanical cleavage: this is the primary method for graphene production. This method use mechanical force to overcome the Val der Waal force between the planes of graphene by adhesive tape. Firstly, graphite flakes are placed between adhesive tape and substrate. The surface is continually and repeatedly peeled causes the cleaved thin graphene flakes adhere to the surface and get fewer layer of graphene [17, 18]. Although, the graphene yield of this method is very low, high quality of graphene without defects is one of advantage. Graphene production by mechanical milling is the later of micromechanical cleavage. Graphite is dispersed in different liquid medium and then low speed milling is performed for exfoliation on graphite. The quality and quantity of graphene is determined by rotation speed, milling ball diameter, milling time, graphene type, solvent, concentration of graphite in solvent and centrifugation speed [19]. However, the drawbacks of this method are the defects on graphene, low yield, high energy consumption and long processing time.

2. Liquid phase exfoliation: this method use ultrasonic or shear force to exfoliate graphite into graphene cooperated with liquid media. To choose the suitable solvent, solvent need to have closely surface energy compared to graphene surface energy in order to reduce the interfacial tension between solvent and graphene planes. Wang et al. [20] estimated the surface energy of graphene to be 46.7 mJm^{-2}. So, Graphite is dispersed in appropriate solvent like N-methyl-2-pyrrolidone (NMP) or N, N-dimethylformamide or o-dichlorobenzene which have surface tensions at 40.8 mJm^{-2}, 37.1 mJm^{-2} and 36.6 mJm^{-2} respectively [21-23] and then ultrasonicate to exfoliate the layers of graphite. During the sonication, the growth and collapse of the micrometer-sized bubbles and voids due to pressure fluctuations induce the graphite exfoliation into graphene sheets [16]. The solvent with a surface energy around 46.7 mJm^{-2} is usually

expensive, corrosive and high boiling point that harmful to health and hard to remove from graphene. However, the exfoliation is unstable with inappropriate solvent such as acetone, water and ethanol that less harmful and easy to evaporate. The cost, simplicity and scalability are the advantages of this method. However, the uncontrollable size and defects on graphene due to excess sonication or shear time are the main drawbacks of this method.

3. Chemical reduction of graphene oxide: the popular method to approach graphene by chemical reduction from graphene oxide to graphene. Firstly, Graphite is intercalated by chemical oxidation to bond the oxygen contained functional groups on the structure of graphene layers. These functional groups maintain the intercalated layer and keep graphene oxide stable in water. This oxidation reaction called Hummer's method [24]. Tour et al. [25] study about how graphite is converted to graphite oxide. They concluded that there are 3 main steps. First, graphite is intercalated with sulfuric acid and oxidized to form graphite oxide. Second, sulfuric acid is reacts with additional potassium permanganate to form dimanganese heptoxide [26]. Third, the sp^2 structure of graphene is destroyed by this harsh chemical reaction from dimanganese heptoxide and appears the oxygen containing functional groups such as hydroxyl or epoxy in the basal plane and carbonyl, carboxylic, phenol and quinone on the edge of plane [26, 27]. The original Hummer's method use sodium nitrate, concentrated sulfuric acid and potassium permanganate as the reactants which are dangerous and not environmental friendly. Some steps of reaction might occur large exothermal causes the explosion or harmful gases form sodium nitrate and phosphoric acid. Thereby, there is some research attempt to eliminate using sodium nitrate for more eco-friendly [28]. In some articles, there are modifications on the steps of Hummer's method for improving

the quality of graphite oxide [29, 30]. Nonetheless, graphite oxidation by Hummer's method introduce defects on graphene structure. The next step to convert graphene oxide to graphene is reduction process. The quality and properties of obtained graphene are depended on this step. There are 3 methods to reduce graphene oxide including chemical, thermal and microwave reduction. For chemical reduction, many kinds of reducing agent are used to reduce oxygen containing group. For example, hydrazine and hydroquinone are used as reducing agent [31, 32] but some researches concern about using green reductants such as L-ascorbic acid and alanine [33, 34]. Thermal reduction at high temperature can also eliminate oxygen containing functional groups from graphene layers by decomposing to carbon dioxide and water [35, 36]. Microwave irradiation is an efficient way for reducing graphene oxide to graphene. Although this method is inexpensive and high productive, the final product quality and chemical toxicity are the main disadvantages.

4. Bottom up synthesis: this is opposite route when compared to other methods. The formation of graphene is generated from organic chemistry which continuous bond to each other. Normally, graphene is synthesized on the substrate atom by atom until become two dimensional structure. Most of researches use benzene containing organic material as a precursor. Jiang et al. [37] promote hexabromobenzene precursor to graphene by mild radical coupling reaction at low temperature. At 220 to 250°C, breaking of C-Br bonding is effective and graphene nanosheet grows on the substrate. Yang et al. [38] produce graphene using linear poly (2, 6-dialkynyl-p-phenylene) as a precursor by alkyne benzannulation. This method is appropriated to produce high quality of graphene. Less product scale and high cost are its drawbacks.

5. Chemical vapor deposition: this method is similar to bottom up synthesis but in gas state. The two reactants in state of gas enter into reaction chamber. The reaction starts when these two reactants are combined together on the heated substrate in the chamber to slowly generate a very thin sheet of nanomaterial. Main reaction for graphene production is pyrolysis on the surface of substrate and carbon atom forming to graphene on the substrate. Zhang et al. [39] describe the decomposition of methane to carbon atom and then dissolve into Nickel film to form a solid solution. Then, the substrate is cooled down and carbon atom diffuse and deposit on Nickel surface to form graphene film. The obtained graphene is very pure with moderate scalability, but expensive and low yield.

6. Electrochemical exfoliation: the principle of this method is reduction and oxidation process. There are 2 types of exfoliation including cathodic and anodic exfoliation. For cathodic exfoliation, electrode attracts with positively charge and cathode show the negative charge that attracts positive ion in solution e.g. Li^+ and exfoliate graphite into graphene. For anodic exfoliation, a positive current withdraws electrons graphite at the anode, so graphite exhibit the positive charge and negative ions in the solution e.g. SO_4^{3-} move into graphite structure causes the interlayer exfoliation [40].

2.4.2 Properties of graphene

For electrical properties, graphene layer can behave as holes and electrons charge carrier. Carbon atoms have four free valence electrons that are available for chemical bonding and three of them bond with other carbon atoms on graphene plane. Therefore, there is one freely remaining electron which available for electrical conduction on above or below graphene sheet. This electron is called pi electron (¶). However, these properties are depended on the number of graphene layers. The

number of layers increasing affect to worse electrical conductivity [16]. The earlier research reported that electron mobility of graphene is extremely high at above 15,000 $cm^2V^{-1}s^{-1}$ to 250,000 $cm^2V^{-1}s^{-1}$ [41]. However, the electron mobility of graphene is effected by graphene quality, temperature and its substrate. For example, Electron mobility is limited to only 40,000 $cm^2V^{-1}s^{-1}$ when use silicon dioxide as a substrate.

For mechanical properties, graphene has an ultimate tensile strength of 130 gigapascals which is stronger than steel and Kevlar around 300 times with ultra-light weight at 0.77 mg/m^3 [42]. Frank et al. measured the Young's modulus of single layer graphene of 0.5 TPa by AFM [43].

For optical properties, one layer of graphene can absorb 2.3% of white light. Amount of graphene layers is almost linearly relative with white light absorption. So, two, three and four layers of graphene are able to absorb light of 4.6, 6.9 and 9.2%, respectively. The maximum light absorption in UV region is at 270 nm [44].

For thermal properties, although the intrinsic thermal conductivity of graphene is very excellent, it is dependent on the method of preparation and defects of graphene. Thermal conductivity of Suspended exfoliated graphene is 2,000-5,000 $Wm^{-1}K^{-1}$ at room temperature [45] but only 600 $Wm^{-1}K^{-1}$ at higher temperature around 660 K [46]. Thermal conductivity of graphene on Silicon dioxide substrate is 600 $Wm^{-1}K^{-1}$ [47].

2.5 Composites

Composites consist of two or more components of organic or inorganic materials. Normally, they consists of two main phases: continuous phase called matrix and discontinuous phase called filler or reinforcement. The major objective of incorporation reinforcement with matrix is to improve some properties of matrix materials. Matrix is classified to three main types: polymer, ceramic and metal. Reinforcing agent is categorized to organic and inorganic material. For example in the case of organic material, wood [48], cellulose fiber [49], carbon nanotube [50] are used as a reinforcing agent. For inorganic reinforcing agent, silica [51], boron carbide [52] are examples.

2.5.1 Types of composite

Types of composite are divided to three types by continuous phase manner.

1. Particle reinforced composites: the continuous phase is dispersed in the matrix for improvement the overall composites. Typically, there many kinds of reinforcing agents such as flake and particle.

2. Fiber reinforced composites: the reinforcing agents have an aspect ratio. There are continuous and discontinuous fiber which align and disperse in the phase of matrix.

3. Structural composites: this composite use combination of different direction of structure such as laminate and sandwich structure. Reinforced phase is separated from matrix phase but physically bond together.

2.5.2 Polymer/graphene nanocomposite

Normally, there are three common methods for combination between polymer and graphene. Each method has different pros and cons. The properties of nanocomposites are related to the method. Therefore, the appropriated method need to be concerned to approach the optimized product.

1. In-situ polymerization: a monomer or low molecular polymer precursor in the solution and graphene are mixed together prior to polymerization. When the polymerization progress, graphene is trapped in the polymer chains. Thereby, homogeneous dispersion and good interaction between graphene and polymer are main advantages. However, the viscosity of system is increased during the polymerization which effect to the difficult of processing. The remaining solvent removal is also the one of problem.

2. Melt blending: molten polymer is mixed graphene to create the composites. The shear force is applied to the polymer and graphene for

mixing at around melting temperature of polymer. The main drawbacks of this technique are poor dispersion and distribution of graphene in the polymer matrix. Moreover, high shear force create the defects on graphene structure.

3. Solution mixing: this method is very simple. First, polymer is dissolved in appropriated solvent and then graphene is added to the solution to mix them together. However, solubility and dispersity of graphene in polymer solution is a concerned problem. The re-aggregation of graphene might occur on the step of solvent evaporation.

Chapter 3

Experiment

3.1 Materials and chemicals

1. Thermoplastic polyester polyurethane (Elastollan®S85A) for extrusion and injection molding was provided by Vinyltec co., Ltd, Thailand.
2. Graphite powder having a particle size of lower than 20 μm was purchased from Sigma-Aldrich, Switzerland.
3. Sulfuric acid 98% (grade AR) were purchased from QRëC, New Zealand.
4. Sodium nitrate (grade AR) were purchased from QRëC, New Zealand.
5. Potassium permanganate (grade AR) was purchased from UNIVAR, New Zealand.
6. Dimethylformamide (grade AR) were purchased from RCI Labscan Limited, Thailand.
7. Acetone (grade CG) were purchased from RCI Labscan Limited, Thailand.
8. Ethanol (grade CG) were purchased from Liquor Distillery Organization, Thailand.
9. L-ascorbic acid 99% (grade AR) was purchased from Vetec, China.
10. Hydrogen peroxide 30% (grade AR) was purchased from Chem-Supply, Australia.
11. Deionized water was purchased from Lee Cier Huad LTD., Thailand.

3.2 Processing machine

1. A twin screw extruder model Thermo prism DSR-28 from LabTech Engineering, Thailand.
2. A wind-up machine was made in-house.
3. A 3D printer of FDM type model Wanhao Duplicator 6, Thailand

3.3 Characterization instruments and testing machines

1. X-ray diffractometer (XRD) model D8 Advance from Bruker, England.
2. Fourier transform infrared spectrometer (FT-IR) model Nicolet 6700 from Thermo Scientific, Germany.
3. Thermogravimetric analyzer (TGA) model TGA/DSC 3^{+} STAR System from Mettler toledo, USA.
4. Differential scanning calorimeter (DSC) model DSC1/STARe from Mettler toledo, USA.
5. Melt flow indexer model 7053 from Kayeness, USA.
6. Hardness durometer shore A from The shore instrument & mfg. Co., Inc., USA
7. Contact angle meter model CAM-PLUS from Tantec Inc., USA
8. Universal testing machine LLOYD, USA
9. Scanning electron microscope (SEM) model JSM-6480LV from JEOL, Japan
10. Picoammeter model 487 from KEITHLEY, USA

3.4 Experimental flow chart

All steps of experiments are described in Figure 3.1

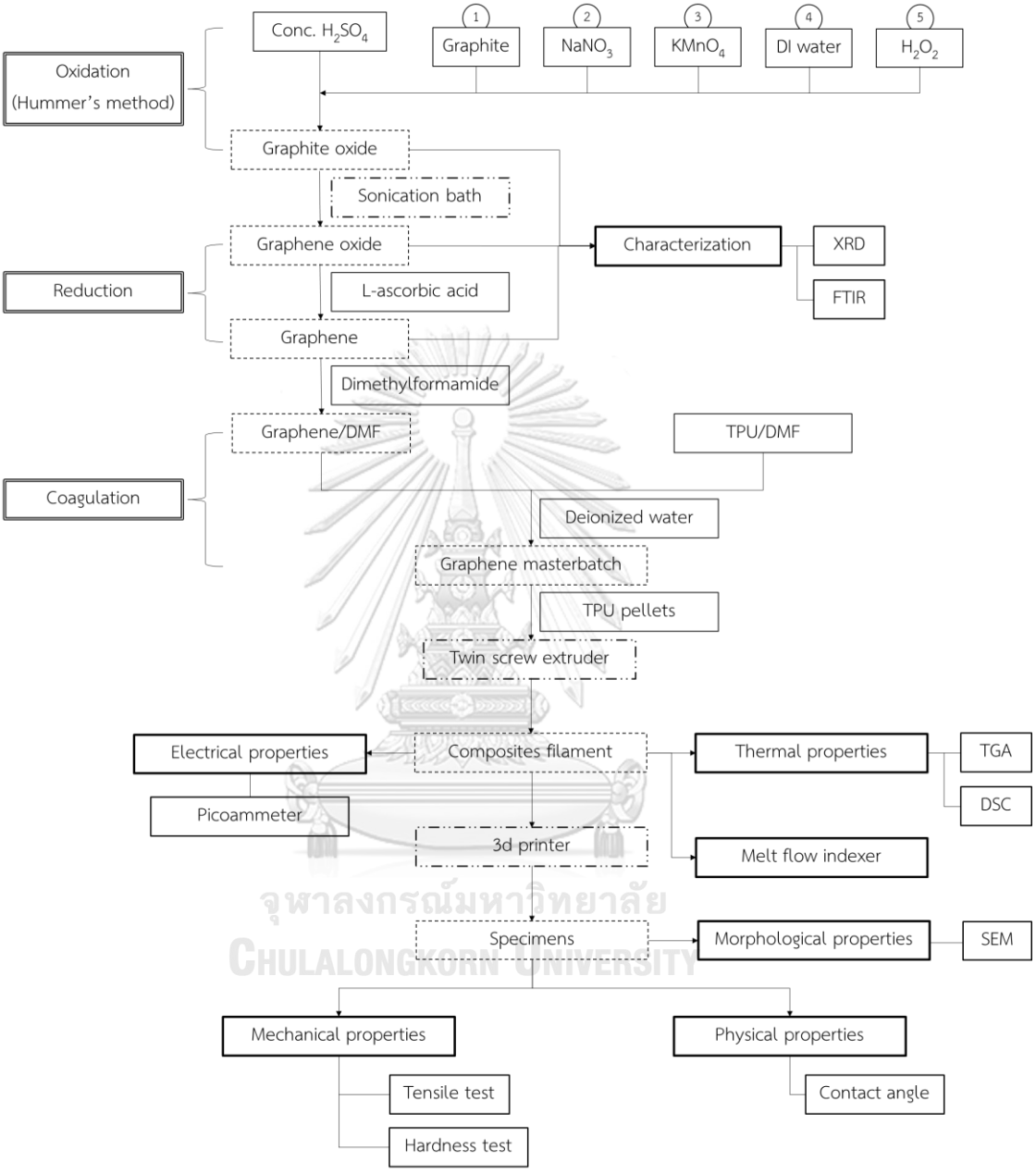

Figure 3.1 Experimental flowchart

3.5 Experimental procedure

3.5.1 Graphene preparation

3.5.1.1 Synthesis of graphite oxide

Graphite oxide was synthesized from graphite flake by oxidation reaction following Hummer's method [53]. First, 9 g of graphite flake and 4.5 g of sodium nitrate ($NaNO_3$) mixture were homogeneously dispersed in 200 ml of sulfuric acid (H_2SO_4) using a magnetic stirrer. The mixture was cooled to 0-10 °C in an ice bath. Then, 27 g of potassium permanganate ($KMnO_4$) was slowly and carefully added while keeping the temperature of the mixture at below 20°C. In this oxidation step, the reaction was conducted for 4 hrs at room temperature. After that, 800 ml of cold deionized water and 10 ml of hydrogen peroxide (H_2O_2) were poured into the mixture to reduce the heat occurring from an exothermal reaction and to remove the unreacted potassium permanganate for 30 min. The mixture neutralization by deionized water by applying centrifugation until pH 5-6. The wetted graphite oxide was placed in a Petri dish and kept in the oven at 45 °C to remove the moisture. Approximately, 8 g of graphite oxide was obtained.

3.5.1.2 Conversion of graphite oxide to graphene

To reduce the Van der Waals force between layers of graphite oxide, ultrasonication was used to separate layers of graphite oxide, 2 g of graphite oxide was dispersed in 1000 ml of deionized water. Then the combining between magnetic stirring and ultrasonication were operated for 3 hrs to obtain graphene oxide.

Graphene oxide was reduced in order to achieve graphene by the chemical method using L-ascorbic acid as a reducing agent. The dispersed graphene oxide in deionized water from the earlier step was chemically reduced by 20 g of L-ascorbic acid. The mixture was continuously stirred for 48 hrs at room temperature. The mixture was maintained to precipitate the black solid graphene at the bottom of a beaker. The colorless aqueous on the upper

was removed prior to vacuum filtration. Graphene was washed with deionized water and ethanol several times to remove residual of L-ascorbic acid. The deionized water was sublimated using a freeze dryer for 24 hrs and solid graphene powder was obtained.

3.5.2 composite filament preparation

3.5.2.1 Masterbatch preparation

The thermoplastic polyurethane was mixed and coagulated with graphene to produce TPU/graphene masterbatch for melt compounding with neat TPU pellets. Briefly, 30 g of TPU was dissolved by 600 ml of dimethylformamide with constant stirring until completely dissolved. To produce the composites, the TPU solution was separated into 4 portions including 60 ml, 120 ml, 180 ml, and 240 ml and graphene was also dispersed in dimethylformamide which divided to 4 portions consist of 0.15 g, 0.30 g, 0.45 g, and 0.60 g of graphene in 10 ml, 20 ml, 30 ml, and 40 ml to create 4 formulas of composites with 0.05%, 0.10%, 0.15%, and 0.20% of graphene, respectively. These two mixtures were mixed together and co-precipitated by dropping into the deionized water. Composites masterbatch was dried in an oven at 90°C for 2 hrs to remove the remaining solvent.

3.5.2.2 Composite filaments preparation

Neat TPU and masterbatch were melt compounded by a twin-screw extruder to produce composites filaments including TPU/0.05G, TPU/0.10G, TPU/0.15G, and TPU/0.20G. Moreover, TPU was prepared as a reference for comparing with composites filament. The temperature profile through the twin screw extruder was 186, 191, 196, 196, and 191°C with an approximately screw speed at 30 rpm. The filaments were extruded with a constant wind-up system to control the diameter of filaments at around 1.75 mm for use with a 3D printer.

Figure 3.2 Twin screw extruder model Prism DSR-28

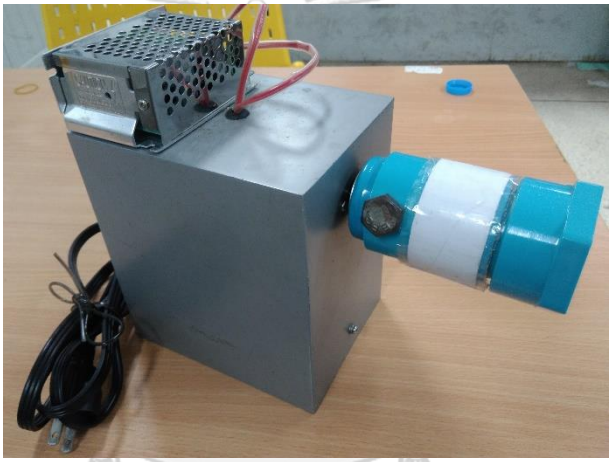

Figure 3.3 in-house wind-up machine

3.5.3 3D printing fabrication

3.5.3.1 program design

The specimen was designed by 123D Design and set the printing conditions by Ultimaker Cura 3.3.1.

3.5.3.2 Specimen printing

The filaments from a twin-screw extruder were printed by fused deposition modeling (FDM) 3D printer, Wanhao Duplicator 6. The printing angle was 90° and 0° with extra coarse quality (nozzle diameter at 0.6 mm) from layer

by layer upon the flat build platform. The controlled variables of printing were described in Table 3.1.

Table 3.1 Controlled variables for 3D printing

Controlled variable	Value
Printing orientation	90°/0°
Nozzle diameter	0.6 mm
Layer height	0.5 mm
Line width	0.5 mm
Wall thickness	10.0 mm
Infill density	100% (line)
Print speed	7 mm/s
Nozzle temperature	227 ℃
Bed temperature	40 ℃

Figure 3.4 3D printer model Wanhao Duplicator 6

3.6 Characterization and testing

3.6.1 X-ray diffractometry, XRD

Characteristic peaks of graphite, graphite oxide, and graphene were analyzed by X-ray diffractometer (Bruker AXS D8 Advance X-ray diffractometer) from the diffraction angle of 5-60° with CuK_{α} radiation at a scanning rate of 2.4°/min to approve the structural difference between three graphene-based materials.

Figure 3.5 X-ray diffractometer (Bruker AXS D8 Advance X-ray diffractometer)

3.6.2 Fourier transform infrared spectrometry, FT-IR

Graphite, graphite oxide and graphene were pressured with KBr to examine the changes of functional groups by Fourier transform infrared spectrometer (Thermo Scientific model Nicolet 6700). Spectrums were received within the wavenumber of 4000 to 400 cm^{-1} at number of sample scans of 64.

Figure 3.6 Fourier transform infrared spectrometer (Thermo Scientific model Nicolet 6700)

3.6.3 Differential scanning calorimetry, DSC

All samples were examined using a differential scanning calorimeter (Mettler Toledo, DSC 1 STAR System). There were 3 steps of identifications including the first heating step, first cooling step, and second heating step. The data from the first cooling step and second heating step were selected to examine the results. Each step was performed within a temperature range from 30 to 250°C in dynamic or non-isothermal mode at a constant heating and cooling rate of 10°C/min under a constant nitrogen gas flow rate of 40 ml/min.

Figure 3.7 Differential scanning calorimeter (Mettler Toledo, DSC 1 STAR System)

3.6.4 Thermogravimetric analysis, TGA

A thermogravimetric analyzer (Mettler Toledo, TGA/DSC 3+ STAR System) was performed to investigate the thermal degradation behavior of all samples. All samples were heated from 50 to 700℃ at a heating rate of 10℃ under the nitrogen atmosphere.

Figure 3.8 Thermogravimetric analyzer (Mettler Toledo, TGA/DSC 3^{+} STAR System)

3.6.5 Melt flow index, MDI

Melt flow index of all samples was measured by Melt flow indexer (Kayeness, model 7053). The measurements were performed at 190℃ with the constant weight of 2.160 g following ASTM D1238. The measurement included 3 batches for each formula.

Figure 3.9 Melt flow indexer (model 7053)

3.6.6 Shore A hardness test

Hardness of all specimen was measures by Hardness durometer Shore A (Shore). The measurement was performed following ASTM D2240. The average of 5 different point's measurement for each sample was reported.

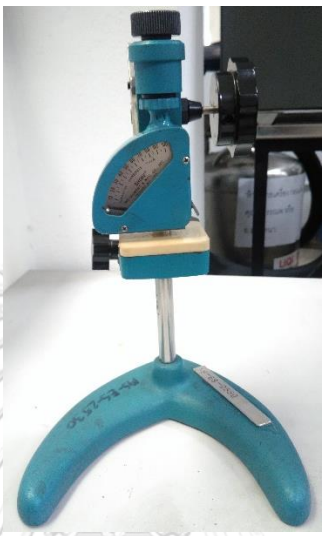

Figure 3.10 Hardness durometer Shore A (Shore)

3.6.7 Contact angle

Contact angle meter (CAM-PLUS Tantec) was used to determine the suface polarity of TPU and nanocomposites specimen. The measurement was done by dropping water on the specimen surface upto 5 points and the average was calculated.

Figure 3.11 Contact angle meter (model CAM-PLUS)

3.6.8 Tensile test

All specimens were fabricated up to 3 pieces for each formula and tested by Universal testing machine following ASTM D412. Testing was operated at a crosshead speed of 150 mm/min with 1 kN of load cell.

Figure 3.12 Universal testing machine (model H10KM)

3.6.9 Scanning electron microscopy

Morphological properties of all samples were inspected by a scanning electron microscope (JEOL JSM-6480LV) at an accelerating voltage of 15kV. All specimens were broken after immersed in liquid nitrogen. The magnification of images were 1500 and 5000 times.

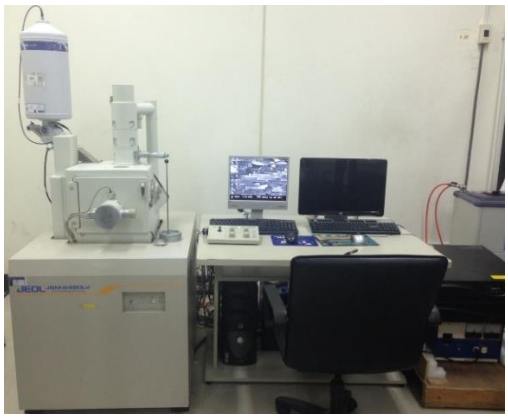

Figure 3.13 Scanning electron microscope (JEOL JSM-6480LV)

3.6.10 Electrical conductivity

Electrical conductivity of TPU and nanocomposites filaments were calculated from resistance. The resistance of filaments were received from current source with fixing voltage at 10 Volt. The filaments were fixed the length of 1 cm and measured the diameter to calculate with the obtained resistance from high resistance meter.

Figure 3.14 High resistance meter (Agilent model 4339B)

Chapter 4

Results and discussions

4.1 Characterization of graphite, graphite oxide and graphene

4.1.1 X-ray diffractometry

X-ray diffractometer was performed to obverse the change of graphene based materials during the chemical treatment. At first, graphite was chemically oxidized by the coordination between sulfuric acid, sodium nitrate and potassium permanganate that cause the existence of oxygen containing functional groups those are hydroxyl, carboxyl, carbonyl, epoxy and phenol groups on basal and edge of graphene layers [28, 36, 53]. As illustrated in Figure 4.1, intercalation between graphene layers was occurred and the distance of graphene layers was increased that relate to shifting from (002) reflection of parent graphite sharp peak at 2θ = 26.58° to (001) reflection of graphite oxide at 2θ =11.34° [54]. The decreasing of 2θ means that the d-spacing between two layers of graphene increased. The d-spacing between graphene layers of graphite compared to graphite oxide was 0.344 and 0.783 respectively. During the reduction process, graphene oxide was converted to graphene using L-ascorbic acid as a reducing agent. The characteristic peak of graphite oxide at 2θ = 11.34° was disappeared after the reduction implying that the oxygen containing functional groups are no longer exist on the graphite oxide sheet anymore [55]. However, there is the appearance of very low intensity of broaden peak around 2θ = 25° which shifted from pristine graphite peak at 2θ = 26.58°. This result refers to the short range ordering of stacked graphene [56] and the shifting of peak to lower degree indicating that there are some oxygen containing functional groups residue or structural defects [57].

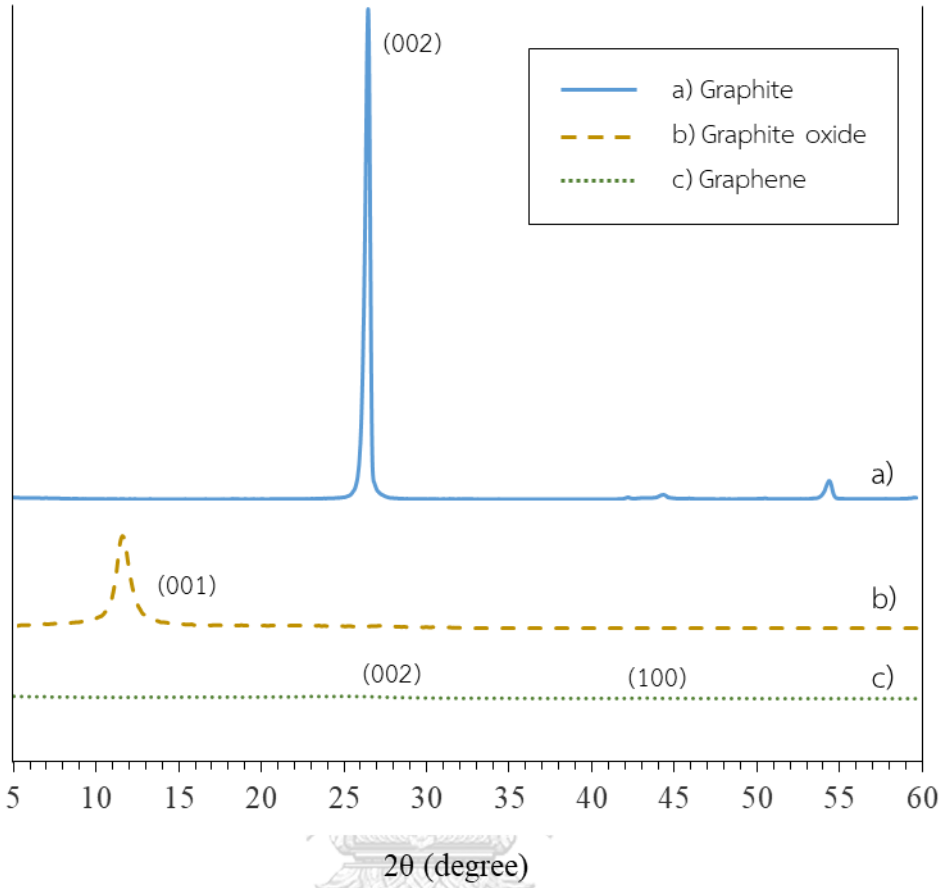

Figure 4.1 X-ray diffractrogram of a) graphite, b) graphite oxide, c) graphene.

4.1.2 Fourier transform infrared spectroscopy

To confirm the differentiation of intermediates during the oxidation and reduction process, graphite, graphite oxide and graphene were investigated by FTIR. Figure 4.2 showed that the FTIR spectra from the pristine graphite does not show any peaks indicated the absence of functional groups on graphite structure [58]. The appearance of significant peaks after the oxidation process of graphite such as very board peak of O-H stretching of OH and COOH functional group around 3381 cm^{-1}, C=O stretching of carbonyl and carboxyl groups at 1,721 cm^{-1}, C=C stretching of unoxidized carbon at 1,618 cm^{-1}, O-H deformation at 1,394 cm^{-1}, C-O-C stretching of epoxide groups at 1,222 cm^{-1} and C-O-H stretching of alkoxy groups at 1,055 cm^{-1} [53, 58]. The decline and disappearance of some peaks after reducing graphene with L-ascorbic acid

such as O-H stretching, C=C stretching and C-O stretching demonstrating that there are few remaining oxygen containing groups on the graphene structure [53].

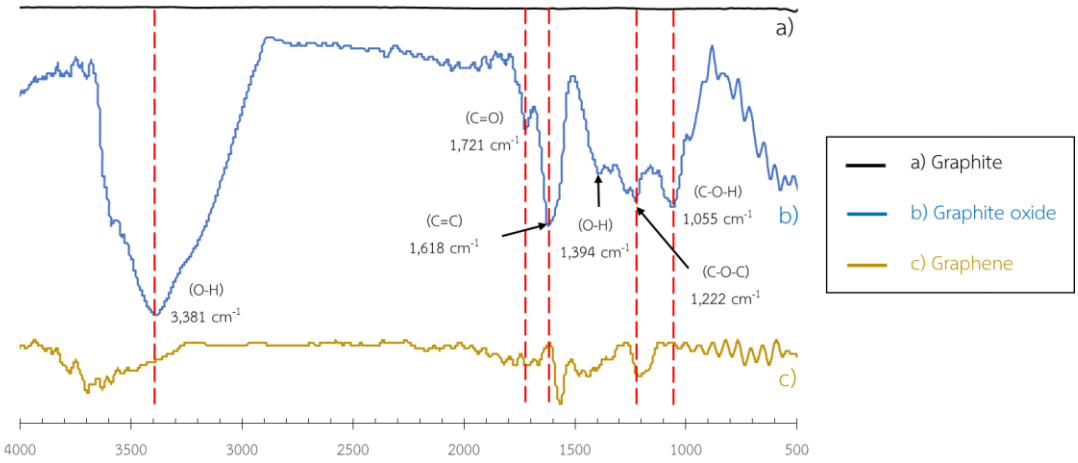

Figure 4.2 FTIR spectra of a) graphite, b) graphite oxide, c) graphene.

4.2 Materials characterization

4.2.1 Differential scanning calorimetry

DSC was performed to evaluate the effect of graphene loading on thermal behaviors of nanocomposites. The cooling step and second heating step were chosen to investigate as illustrated in Figure 4.3 and Figure 4.4, respectively. When consider the cooling step, crystallization temperature (T_c) was separated into two ranges and broaden with shifting to higher temperature. From this result, it might be the effect of graphene on crystallization of hard segment which induced higher crystallization rate than pure TPU. However, degree of crystallinity of TPU which observed from peak area was not affected by the graphene adding. In the case of thermal behavior of heating step from Table 4.1, the increasing of melting temperature (T_m) depended on graphene induced TPU chains to form more stable crystalline or larger size [59, 60]. However, the heat of fusion during melting crystalline step decreased when graphene was added which affected to the decrement of TPU's crystallinity.

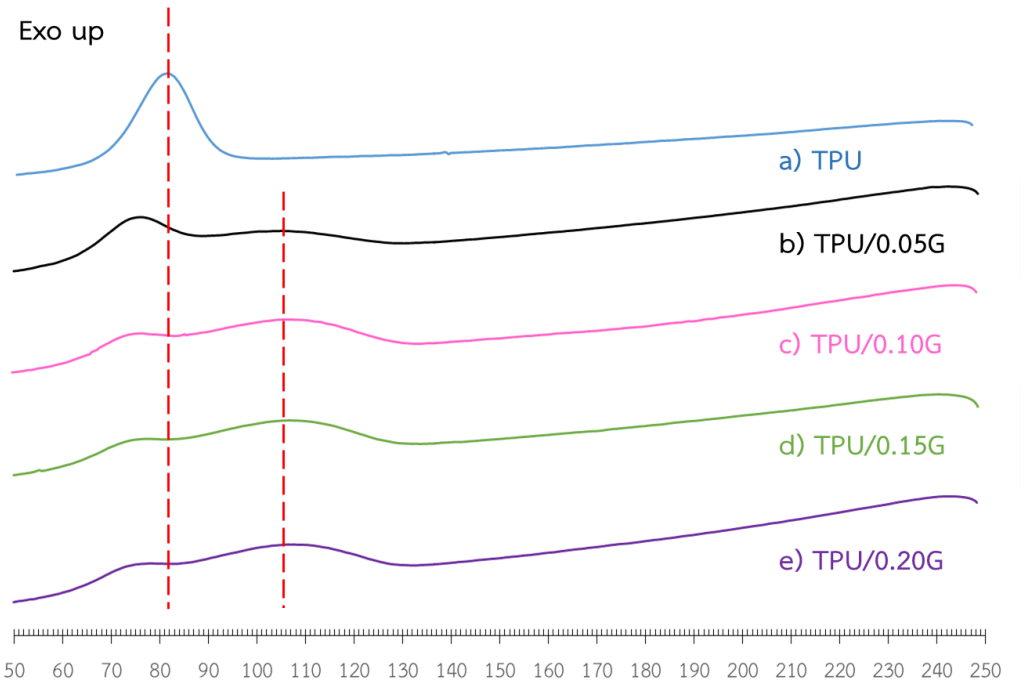

Figure 4.3 DSC thermograms of a) TPU and nanocomposites with b) 0.05, c) 0.10, d) 0.15 and e) 0.20 wt% of graphene at cooling step.

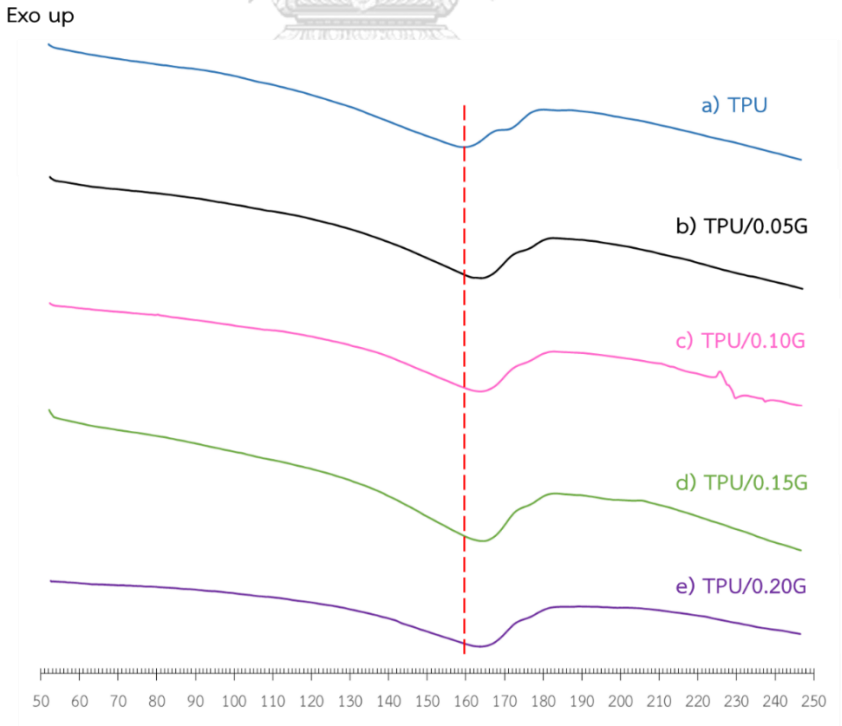

Figure 4.4 DSC thermograms of a) TPU and nanocomposites with b) 0.05, c) 0.10, d) 0.15 and e) 0.20 wt% of graphene at second heating step.

Table 4.1 Melting temperature of TPU and nanocomposites.

Formula	Melting temperature, T_m (°C)	Heat of fusion (J/g)
TPU	158.4	9.3
TPU/0.05G	161.4	8.1
TPU/0.10G	163.1	7.5
TPU/0.15G	163.4	8.1
TPU/0.20G	163.5	8.0

4.2.2 Thermal gravimetric analysis

The effects of graphene on thermal stability of TPU was studied. TGA thermogram as demonstrated in Figure 4.5 shows two steps of thermal degradation. The first and second degradation consecutively refer to soft and hard segment decomposition, respectively. From Table 4.2, the first degradation of all nanocomposites were slightly higher than TPU due to the effect of physical interaction between graphene and soft segment of TPU that lead to the restriction of TPU chain movement during degradation [61, 62]. The second decomposition of nanocomposites slightly increased compared to TPU due to the restriction of graphene in the hard domain of TPU. However, the percentage of residue was not clearly explain about the effect of graphene on TPU.

Table 4.2 Thermal properties of TPU and nanocomposites by TGA.

Formula	Temperature of 1^{st} step degradation (°C)	Temperature of 2^{nd} step degradation (°C)	%residue
TPU	335.3	411.0	7.55
TPU/0.05G	336.3	411.0	9.19
TPU/0.10G	337.2	411.3	8.45
TPU/0.15G	338.0	412.7	7.66
TPU/0.20G	338.0	414.3	7.99

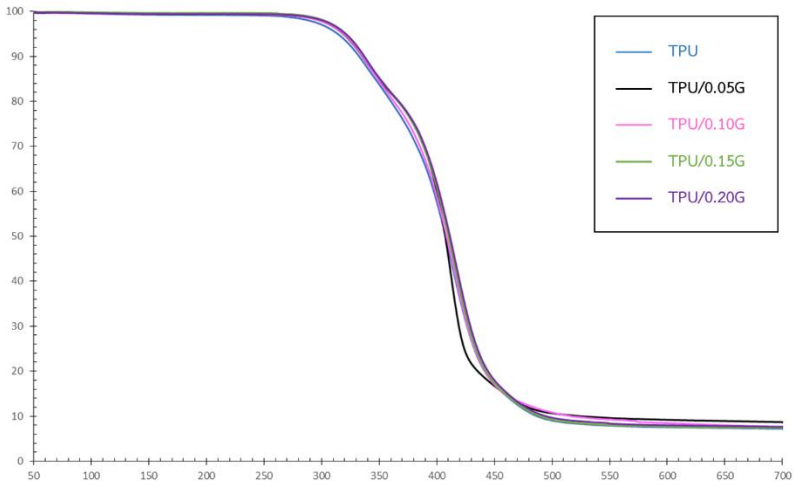

Figure 4.5 TGA thermogram of TPU and nanocomposites.

4.2.3 Melt flow index

The effect of graphene on extrinsic viscosity within the molten state at fixed melting temperature is shown in Figure 4.6. The melt flow index at 190°C with 2.160 kg loading of TPU, TPU/0.05G, TPU/0.10G, TPU/0.15G and TPU/0.20G were 4.8, 4.0, 3.5, 3.4, and 3.0 respectively. When the graphene loading increased, the melt viscosity of the composites increased due to the movement of polymer chains during melting is restrained by the existence of graphene which causes the slower mobility through the die or increasing viscosity of bulk materials [63]. The mean difference of all samples are not significant except TPU/0.10G and TPU/0.15G which observing from statistic calculations.

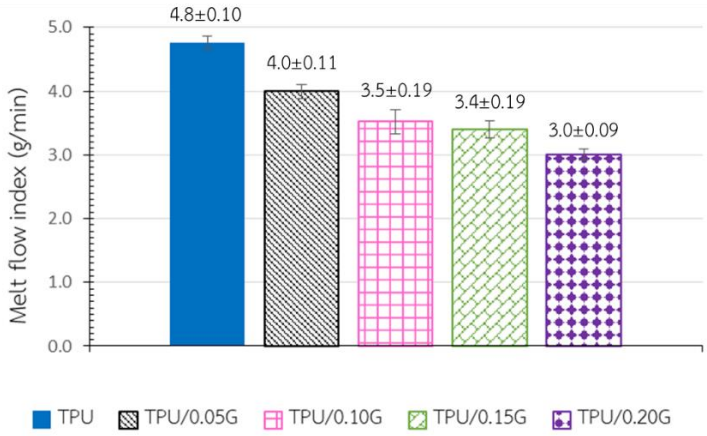

Figure 4.6 Melt flow index of TPU and nanocomposites.

4.2.4 Hardness

The hardness durometer shore A was carried out to measure the hardness of elastic materials including TPU and TPU/graphene composites by indention. This measurement sometimes related to determining of the elastic modulus of materials. The hardness of all specimen is exhibited in Figure 4.7. The incorporation of graphene in hard segment of TPU matrix affected to the stiffer materials which induced the higher hardness [54]. However, the hardness of specimen is lower than the explanation in factory's technical data sheet. It might due to the point of indention was located between seam of polymer printing line and the quality of the specimens. Referring to statistic results, the hardness of TPU is increased with graphene adding but level off after graphene is higher than 0.10 percentages.

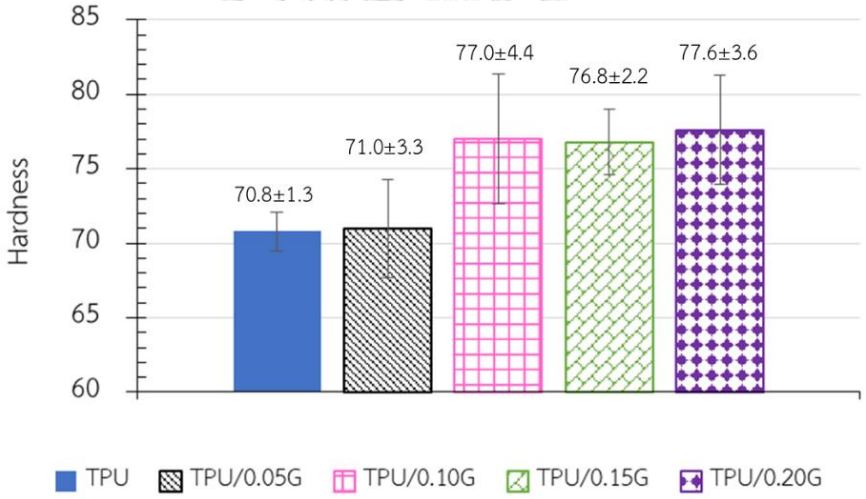

Figure 4.7 Hardness of TPU and nanocomposites.

4.2.5 Contact angle

The hydrophilicity of TPU and TPU/graphene nanocomposites specimens were measured by a contact angle meter using water as a testing liquid. As illustrated in Figure 4.8, the pure TPU is the most hydrophilic compared to other nanocomposites and the increasing of graphene loading instilled more hydrophobicity of materials because the nature of graphene which contain less polar functional groups resulting is hydrophobicity. Therefore, incorporation of graphene with TPU affected to increment

of hydrophobicity or decrement of wettability of materials surface [54]. However, the specimen from 3D printer with extra coarse nozzle diameter (0.6 mm) were not suitable for this measurement due to their unstable or inconsistent surfaces. From the statistic calculations, the mean difference of TPU/0.10G, TPU/0.15G and TPU/0.20G are significant.

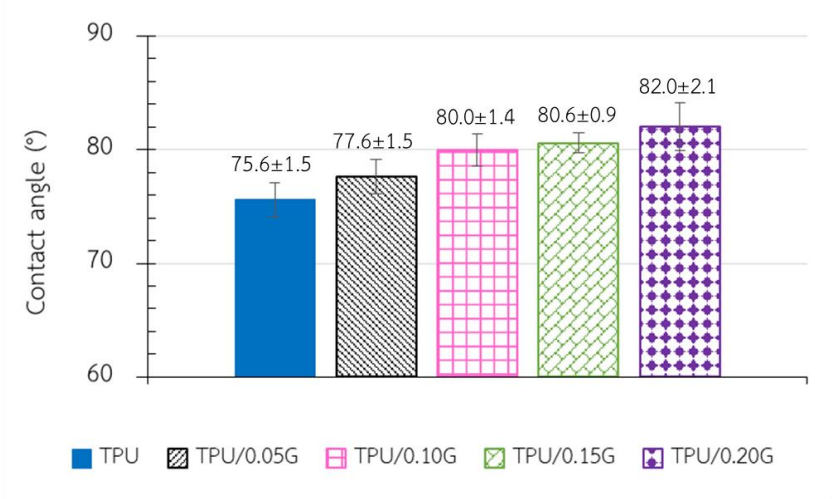

Figure 4.8 Contact angle of TPU and nanocomposites.

4.2.6 Tensile properties

The effects of graphene as a reinforcing agent on mechanical properties of nanocomposites was investigated by the tensile testing. The specimen of all samples were printed by 3D printing with 0°/90° direction following ASTM D412 type D dimension. All specimen were effectively printed except pure TPU specimen due to the hardness of its filament which obstructed the feeding filament to 3D printer. Additionally, the surface of previous printed layer was sometimes peeled off by traveling of nozzle head during printing that cause the incomplete printed specimen. Nevertheless, only one specimen of TPU could be printed and tested. Beside the compatibility of matrix and nanofillers was an important factor on the final product's properties, the dispersion and distribution of nanofillers in the polymer matrix were also crucial variables. However, the existence of defects on specimen from printing

program were a serious problem of stress concentration during stretching which effected to lower tensile strength than actual its strength and become more brittle. According to Figure 4.9 and Figure 4.10, the results showed that tensile stress at 100 mm extension and Young's modulus of all of nanocomposites were better than TPU. TPU/0.05G has a greatest stress compared to other nanocomposites due to the high quality of unbroken printed specimen after stretching as shown in Figure 4.11. The printing potential of TPU depend on material flow during printing. TPU/0.05G was the easiest printable filament. Therefore, the tensile properties of TPU/0.05G was highest among other nanocomposites.

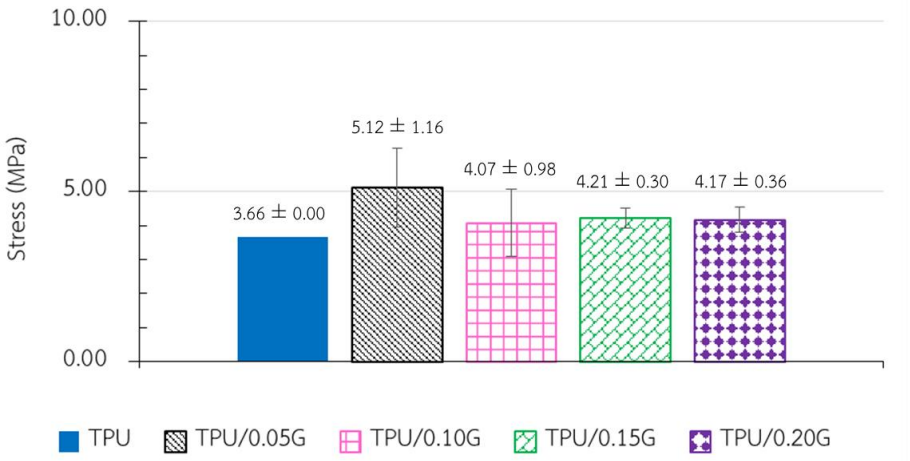

Figure 4.9 Stress at 100 mm extension of TPU and nanocomposites.

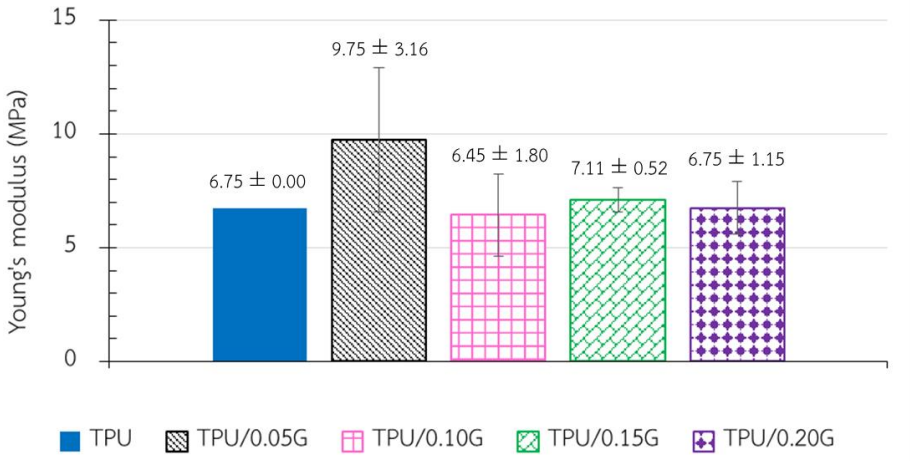

Figure 4.10 Young's modulus of TPU and nanocomposites.

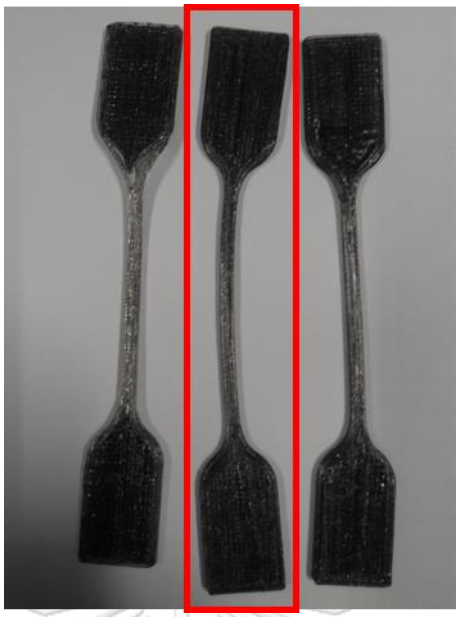

Figure 4.11 Unbroken TPU/0.05G specimens

4.2.7 Scanning electron microscopy

The specimens were frozen by liquid nitrogen and broken by the impact load. The morphology of TPU and nanocomposites was inspected to observe the distribution and dispersion of graphene in TPU matrix. As shown in Figure 4.12, the cracked surface of TPU showed a smoother surface than those of other nanocomposites. The roughness of nanocomposites increased with higher loading of graphene in TPU. The agglomeration was happened after the loading was higher than 0.05 wt%. This result showed that TPU is not compatible with graphene at higher loading. Therefore, the aggregation of graphene affects the mechanical properties of nanocomposites according to the tensile tests.

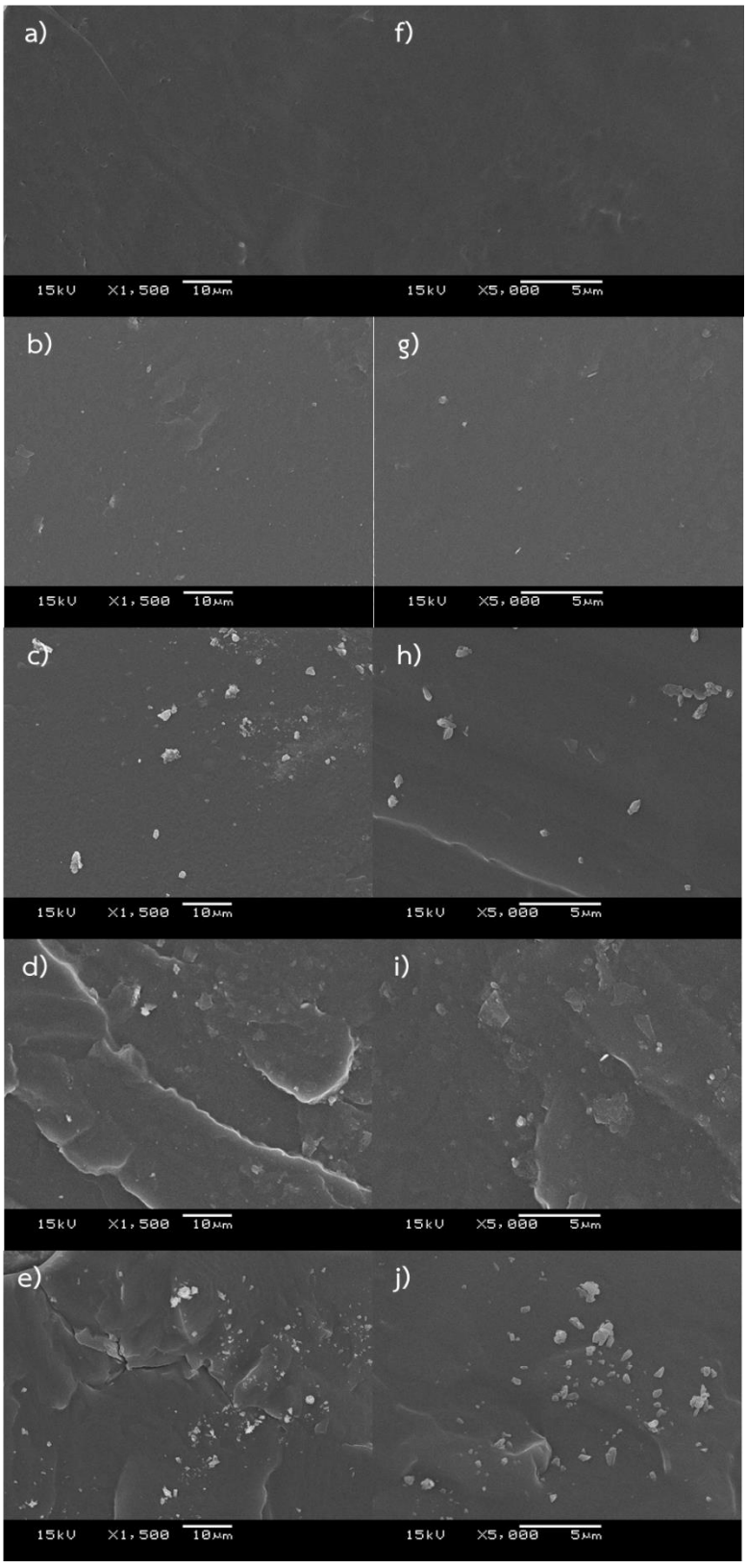

Figure 4.12 Surface morphology image of a),f) TPU, b),g) TPU/0.05G, c),h) TPU/0.10G, d),i) TPU/0.15G and e),j) TPU/0.20G at 1,500 and 5,000 magnification respectively.

4.2.8 Electrical conductivity

Resistance of TPU and TPU/graphene nanocomposites were measured by applying the current into filaments with low voltage fixing at 10 V. The value of resistance of all filaments were read as shown in Figure 4.13. The resistance of TPU was respectively decreased with increase amount of graphene loading. Then, the electrical conductivity of filaments were calculated from the equation as exhibited in Figure 4.14 and the conductivity were demonstrated in Figure 4.15. Length (l) was fixed at 1 cm and diameter was around 1.75 to 1.85 mm. A was cross-sectional area of filament which calculated from diameter. The results showed that graphene could improve the conductivity of TPU but not much due to low amount of graphene. The appearance of graphene cluster induced the tunneling effect of graphene with neighboring graphene which cause to the increment of conductivity [64].

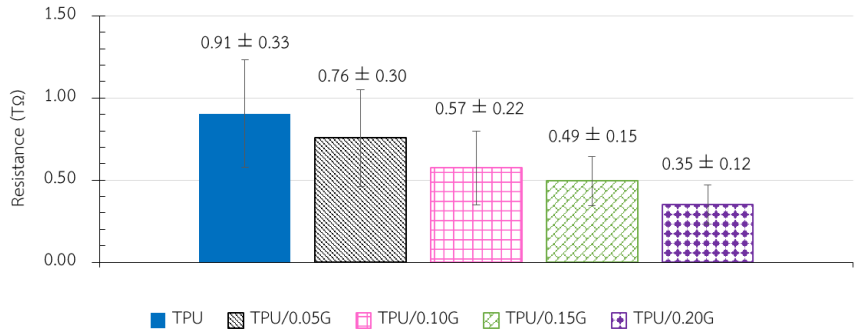

Figure 4.13 Resistance of TPU and nanocomposites.

$$\sigma = \frac{l}{AR}$$

Figure 4.14 Conductivity (σ) equation

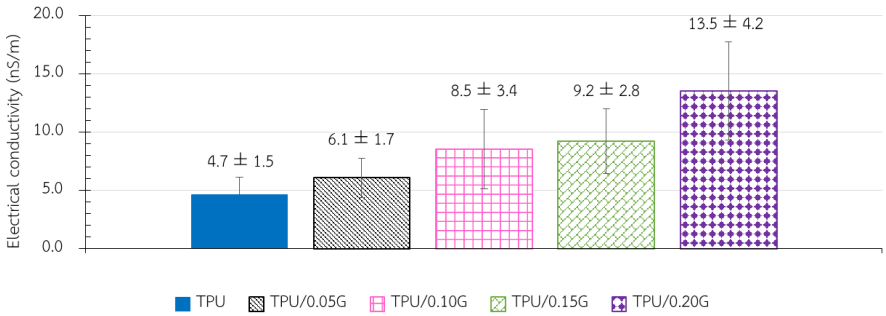

Figure 4.15 Electrical conductivity of TPU and nanocomposites.

Chapter 5

Conclusions and suggestions

5.1 Conclusions

The original filament obtained from thermoplastic polyurethane (Elastollan S85A) of an injection molding grade does not appropriate for 3D printing process. The properties of TPU was then tuned to make it more potentially printable material by using graphene as a nanofillers. Firstly, graphene oxide was prepared from graphite oxidation via modified Hummer's method following by ultrasonication. Graphene is consequently obtained from chemical reduction of graphene oxide by L-ascorbic acid. The TPU 3D printing filament and nanocomposites filament is prepared by a twin screw extruder. For nanocomposites, neat TPU was melt blended with TPU/graphene masterbatch to include the filaments with 0.05, 0.10, 0.15, 0.20 wt% of graphene. TPU and nanocomposites filament are 3D printed to produce the specimen in order to study the possibility of printing.

1. Graphite oxide and graphene synthesis are successful confirmed by FTIR and XRD results
2. Graphene loading affect melting temperature and crystallization temperature of TPU to increase.
3. First and second degradation temperature of TPU increased after incorporation of graphene in TPU.
4. The higher loading of graphene leads to higher viscosity of materials.
5. Hardness of nanocomposites was improved with the increasing amount of graphene loading. The higher loading affects the hardness.
6. The higher weight percentage of graphene adding in TPU affect the hydrophobicity of nanocomposites.
7. The incorporation of graphene into TPU matrix improve the printing efficiency of TPU. The graphene loading at 0.05 wt% gives the most

efficiently printable nanocomposites, considering with the highest quality of specimen.

8. TPU/0.05G shows the highest tensile strength and Young's modulus compared to other nanocomposites.
9. SEM results confirm that, for TPU/0.05G, the graphene is well-dispersed and does not aggregate thus yields the optimum tensile properties.
10. Electrical conductivity of TPU/graphene nanocomposites are improved with larger amount of graphene but the percentage of graphene at 0.20wt% is not enough to change insulated TPU to antistatic TPU nanocomposites.

5.2 Suggestions

1. Blobs and stringing of TPU while printing always occur due to characteristic properties of TPU. The blobs and stringing during printing affect to discontinuous printing that cause defects on specimens or products.
2. Blobs and stringing of TPU are reduced after incorporation of graphene in TPU.
3. The moisture trapping in filaments from water cooling after extrusion induces voids to be occurred in the filaments while TPU is melted through the nozzle. Therefore, the cooling by dry air is one option for reducing moisture inclusion.
4. The hardness of filament is a crucial factor for 3D printing process. The appropriate hardness can drive the filament through nozzle. Thus, the hardness of filament should be improved.
5. The processing temperature of 3D printing nozzle is also a main factor. The most appropriated processing temperature of TPU is 227 °C.
6. The printing speed should not exceed 10 mm/min because at too fast printing speed, polymers may drop and yield unfilled artifacts.
7. The printed TPU surface is always peeled when the nozzle move pass. The addition of graphene into TPU matrix reduces this problem.

REFERENCES

[1] 3DHubs. What is 3d printing? 2018.

[2] Ngo, T.D., Kashani, A., Imbalzano, G., Nguyen, K.T.Q., and Hui, D. Additive manufacturing (3D printing): A review of materials, methods, applications and challenges. Composites Part B: Engineering 143 (2018): 172-196.

[3] Chohan, J.S., Singh, R., Boparai, K.S., Penna, R., and Fraternali, F. Dimensional accuracy analysis of coupled fused deposition modeling and vapour smoothing operations for biomedical applications. Composites Part B: Engineering 117 (2017): 138-149.

[4] Mohamed, O.A., Masood, S.H., and Bhowmik, J.L. Optimization of fused deposition modeling process parameters: a review of current research and future prospects. Advances in Manufacturing 3(1) (2015): 42-53.

[5] Brunello, G., et al. Powder-based 3D printing for bone tissue engineering. Biotechnol Adv 34(5) (2016): 740-753.

[6] Yusuf, B. Types of 3d printing technology. 2018.

[7] Utela, B., Storti, D., Anderson, R., and Ganter, M. A review of process development steps for new material systems in three dimensional printing (3DP). Journal of Manufacturing Processes 10(2) (2008): 96-104.

[8] Wang, X., Jiang, M., Zhou, Z., Gou, J., and Hui, D. 3D printing of polymer matrix composites: A review and prospective. Composites Part B: Engineering 110 (2017): 442-458.

[9] Chakravorty, D. what is stl file format extension 3d printing. 2017.

[10] Richard J. Spontak and Patel, N.P. Thermoplastic elastomers fundamentals and applications. Current opinion in colloid & interface science 5 (2000): 334-341.

[11] Mehdi Barikani and Barmar, M. Thermoplastic Polyurethane Elastomers: Synthesis, and Study of Effective Structural Parameters. Iranian Polymer Journal 5 (1996): 231-235.

[12] Qi, H.J. and Boyce, M.C. Stress–strain behavior of thermoplastic polyurethanes. Mechanics of Materials 37(8) (2005): 817-839.

[13] Singh, V., Joung, D., Zhai, L., Das, S., Khondaker, S.I., and Seal, S. Graphene based materials: Past, present and future. Progress in Materials Science 56(8) (2011): 1178-1271.

[14] Fasolino, A., Los, J.H., and Katsnelson, M.I. Intrinsic ripples in graphene. Nat Mater 6(11) (2007): 858-61.

[15] A. K. GEIM and NOVOSELOV, K.S. The rise of graphene. Nature materials 6 (2007): 183-191.

[16] Phiri, J., Gane, P., and Maloney, T.C. General overview of graphene: Production, properties and application in polymer composites. Materials Science and Engineering: B 215 (2017): 9-28.

[17] G. Sh. SHMAVONYAN, G.G. SEVOYAN, and AROUTIOUNIAN, V.M. ENLARGING THE SURFACE AREA OF MONOLAYER GRAPHENE SYNTHESIZED BY MECHANICAL EXFOLIATION. Armenian Journal of Physics 6(1) (2013): 1-6.

[18] Dresselhaus, M.S. and Dresselhaus, G. Intercalation compounds of graphite. Advances in Physics 51(1) (2002): 1-186.

[19] Zhao, W., Fang, M., Wu, F., Wu, H., Wang, L., and Chen, G. Preparation of graphene by exfoliation of graphite using wet ball milling. Journal of Materials Chemistry 20(28) (2010).

[20] Wang, S., Zhang, Y., Abidi, N., and Cabrales, L. Wettability and surface free energy of graphene films. Langmuir 25(18) (2009): 11078-81.

[21] Parvez, K., Yang, S., Feng, X., and Müllen, K. Exfoliation of graphene via wet chemical routes. Synthetic Metals 210 (2015): 123-132.

[22] Christopher E. Hamilton, Jay R. Lomeda, Zhengzong Sun, James M. Tour, and Barron, A.R. High-Yield Organic Dispersions of Unfunctionalized Graphene. Nano letters 9 (2009): 3460-3462.

[23] Hernandez, Y., et al. High-yield production of graphene by liquid-phase exfoliation of graphite. Nat Nanotechnol 3(9) (2008): 563-8.

[24] William S. Hummers and Offeman, R.E. Preparation of graphitic oxide. 1958. 1339.

[25] Ayrat M. Dimiev and Tour, J.M. Mechanism of Graphene Oxide Formation. ACS Nano 8 (2014): 3060-3068.

[26] Dreyer, D.R., Park, S., Bielawski, C.W., and Ruoff, R.S. The chemistry of graphene oxide. Chem Soc Rev 39(1) (2010): 228-40.

[27] Kim, F., Cote, L.J., and Huang, J. Graphene oxide: surface activity and two-dimensional assembly. Adv Mater 22(17) (2010): 1954-8.

[28] Chen, J., Yao, B., Li, C., and Shi, G. An improved Hummers method for eco-friendly synthesis of graphene oxide. Carbon 64 (2013): 225-229.

[29] Muzyka, R., Kwoka, M., Smędowski, Ł., Díez, N., and Gryglewicz, G. Oxidation of graphite by different modified Hummers methods. New Carbon Materials 32(1) (2017): 15-20.

[30] Zaaba, N.I., Foo, K.L., Hashim, U., Tan, S.J., Liu, W.-W., and Voon, C.H. Synthesis of Graphene Oxide using Modified Hummers Method: Solvent Influence. Procedia Engineering 184 (2017): 469-477.

[31] Guoxiu Wang, et al. Facile Synthesis and Characterization of Graphene Nanosheets. The Journal of Physical Chemistry 112 (2008): 8192-8195.

[32] Tung, V.C., Allen, M.J., Yang, Y., and Kaner, R.B. High-throughput solution processing of large-scale graphene. Nat Nanotechnol 4(1) (2009): 25-9.

[33] De Silva, K.K.H., Huang, H.H., Joshi, R.K., and Yoshimura, M. Chemical reduction of graphene oxide using green reductants. Carbon 119 (2017): 190-199.

[34] Wang, J., Salihi, E.C., and Siller, L. Green reduction of graphene oxide using alanine. Mater Sci Eng C Mater Biol Appl 72 (2017): 1-6.

[35] Vallés, C., David Núñez, J., Benito, A.M., and Maser, W.K. Flexible conductive graphene paper obtained by direct and gentle annealing of graphene oxide paper. Carbon 50(3) (2012): 835-844.

[36] Eigler, S., Grimm, S., Enzelberger-Heim, M., Muller, P., and Hirsch, A. Graphene oxide: efficiency of reducing agents. Chem Commun (Camb) 49(67) (2013): 7391-3.

[37] Jiang, L., et al. Low-temperature, bottom-up synthesis of graphene via a radical-coupling reaction. J Am Chem Soc 135(24) (2013): 9050-4.

[38] Yang, W., Lucotti, A., Tommasini, M., and Chalifoux, W.A. Bottom-Up Synthesis of Soluble and Narrow Graphene Nanoribbons Using Alkyne Benzannulations. J Am Chem Soc 138(29) (2016): 9137-44.

[39] YI ZHANG, LUYAO ZHANG, and ZHOU, C. Review of Chemical Vapor Deposition of Graphene and Related Applications. Accounts of Chemical Research 46 (2012): 2329-2339.

[40] Yu, P., Lowe, S.E., Simon, G.P., and Zhong, Y.L. Electrochemical exfoliation of graphite and production of functional graphene. Current Opinion in Colloid & Interface Science 20(5-6) (2015): 329-338.

[41] Bolotin, K.I., et al. Ultrahigh electron mobility in suspended graphene. Solid State Communications 146(9-10) (2008): 351-355.

[42] Changgu Lee, Xiaoding Wei, Jeffrey W. Kysar, and Hone, J. Measurement of the Elastic Properties and Intrinsic Strength of Monolayer Graphene. Science 321 (2008): 385-388.

[43] I. W. Frank, D. M. Tanenbaum, A. M. van der Zande, and McEuen, P.L. Mechanical properties of suspended graphene sheet. Journal of Vacuum Science & Technology B: Microelectronics and Nanometer Structures Processing, Measurement, and Phenomena (2007): 2558-2561.

[44] Bae, S., et al. Roll-to-roll production of 30-inch graphene films for transparent electrodes. Nat Nanotechnol 5(8) (2010): 574-8.

[45] Alexander A. Balandin, et al. Superior Thermal Conductivity of Single-Layer Graphene. Nano letters 8 (2008): 902-907.

[46] Clement Faugeras, Blaise Faugeras, Milan Orlita, M. Potemski, Rahul R. Nair, and Geim, A.K. Thermal Conductivity of Graphene in Corbino Membrane Geometry. ACS Nano 4 (2010): 1889-1892.

[47] Jae Hun Seol, et al. Two-Dimensional Phonon Transport in Supported Graphene. Science 328 (2010): 213-216.

[48] Moreno, D.D.P., Hirayama, D., and Saron, C. Accelerated aging of pine wood waste/recycled LDPE composite. Polymer Degradation and Stability 149 (2018): 39-44.

[49] Hadjadj, A., et al. Effects of cellulose fiber content on physical properties of polyurethane based composites. Composite Structures 135 (2016): 217-223.

[50] Xiao, K., Zhang, L., and Zarudi, I. Mechanical and rheological properties of carbon nanotube-reinforced polyethylene composites. Composites Science and Technology 67(2) (2007): 177-182.

[51] Jeziorska, R., Szadkowska, A., Zielecka, M., Wenda, M., and Kepska, B. Morphology and thermal properties of HDPE nanocomposites: Effect of spherical silica surface modification and compatibilizer. Polymer Degradation and Stability 145 (2017): 70-78.

[52] Soltani, Z., Beigzadeh, A., Ziaie, F., and Asadi, E. Effect of particle size and percentages of Boron carbide on the thermal neutron radiation shielding properties of HDPE/B4C composite: Experimental and simulation studies. Radiation Physics and Chemistry 127 (2016): 182-187.

[53] Daniela C. Marcano, et al. Improved Synthesis of Graphene Oxide. ACS Nano 4 (2010): 4806-4814.

[54] Bera, M. and Maji, P.K. Effect of structural disparity of graphene-based materials on thermo-mechanical and surface properties of thermoplastic polyurethane nanocomposites. Polymer 119 (2017): 118-133.

[55] Ahmed A. Elzatahry, et al. Nanocomposite Graphene-Based Material for Fuel Cell Applications. International Journal of Electrochemical Science 7 (7): 3115-3126.

[56] Changjing Fu, Guogang Zhao, Haijun Zhang, and Li, S. Evaluation and characterization of reduced graphene oxide nanosheets as anode materials for lithium-ion batteries. International Journal of Electrochemical Science 8 (2013): 6269-6280.

[57] Gao, W., Alemany, L.B., Ci, L., and Ajayan, P.M. New insights into the structure and reduction of graphite oxide. Nat Chem 1(5) (2009): 403-8.

[58] Mai, T.T., Ha Thuc, C.N., and Thuc, H.H. Preparation of Graphene Nano-Layer by Chemical Graphitization of Graphite Oxide from Exfoliation and Preliminary Reduction. Fullerenes, Nanotubes and Carbon Nanostructures 23(8) (2015): 742-749.

[59] Strankowski, M., Korzeniewski, P., Strankowska, J., A, S.A., and Thomas, S. Morphology, Mechanical and Thermal Properties of Thermoplastic Polyurethane Containing Reduced Graphene Oxide and Graphene Nanoplatelets. Materials (Basel) 11(1) (2018).

[60] Thakur, S. and Karak, N. Ultratough, Ductile, Castor Oil-Based, Hyperbranched, Polyurethane Nanocomposite Using Functionalized Reduced Graphene Oxide. ACS Sustainable Chemistry & Engineering 2(5) (2014): 1195-1202.

[61] Zhang, J., Zhang, C., and Madbouly, S.A. In situ polymerization of bio-based thermosetting polyurethane/graphene oxide nanocomposites. Journal of Applied Polymer Science 132(13) (2015): 1-8.

[62] Thakur, S. and Karak, N. A tough, smart elastomeric bio-based hyperbranched polyurethane nanocomposite. New Journal of Chemistry 39(3) (2015): 2146-2154.

[63] Noorunnisa Khanam, P., et al. Melt processing and properties of linear low density polyethylene-graphene nanoplatelet composites. Vacuum 130 (2016): 63-71.

[64] Khanam, P.N., Ponnamma, D., and AL-Madeed, M.A. Electrical Properties of Graphene Polymer Nanocomposites. in Sadasivuni, K.K., Ponnamma, D., Kim, J., and Thomas, S. (eds.),Graphene-Based Polymer Nanocomposites in Electronics, pp. 25-47. Cham: Springer International Publishing, 2015.

APPENDIX

Appendix a Fourier transform infrared spectroscopy, FTIR

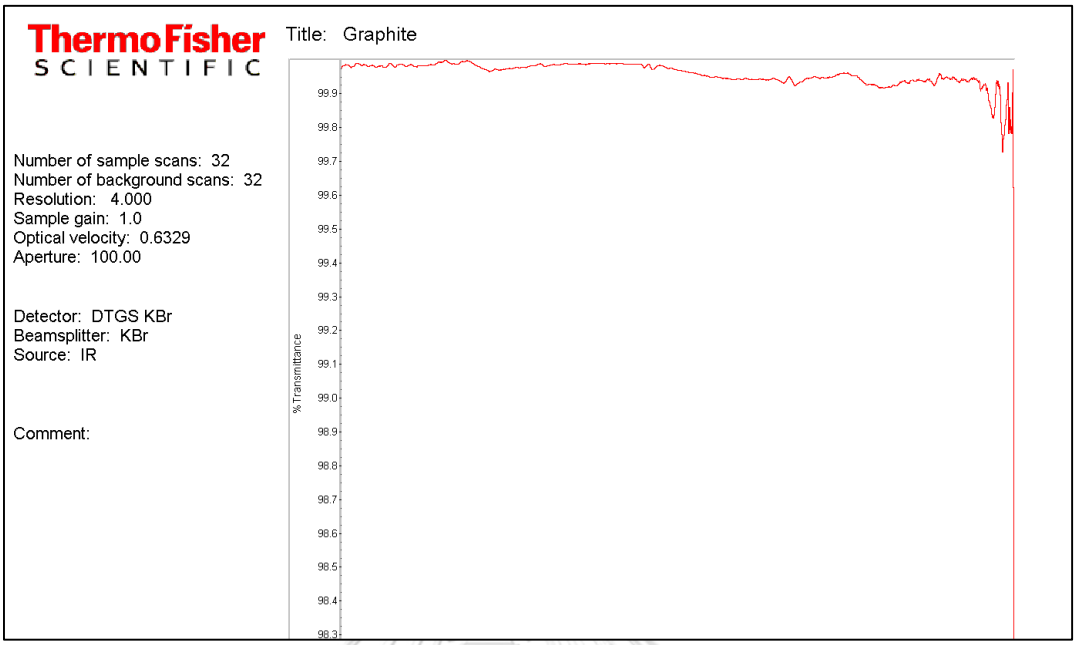

Figure a.1 FTIR spectrum of graphite

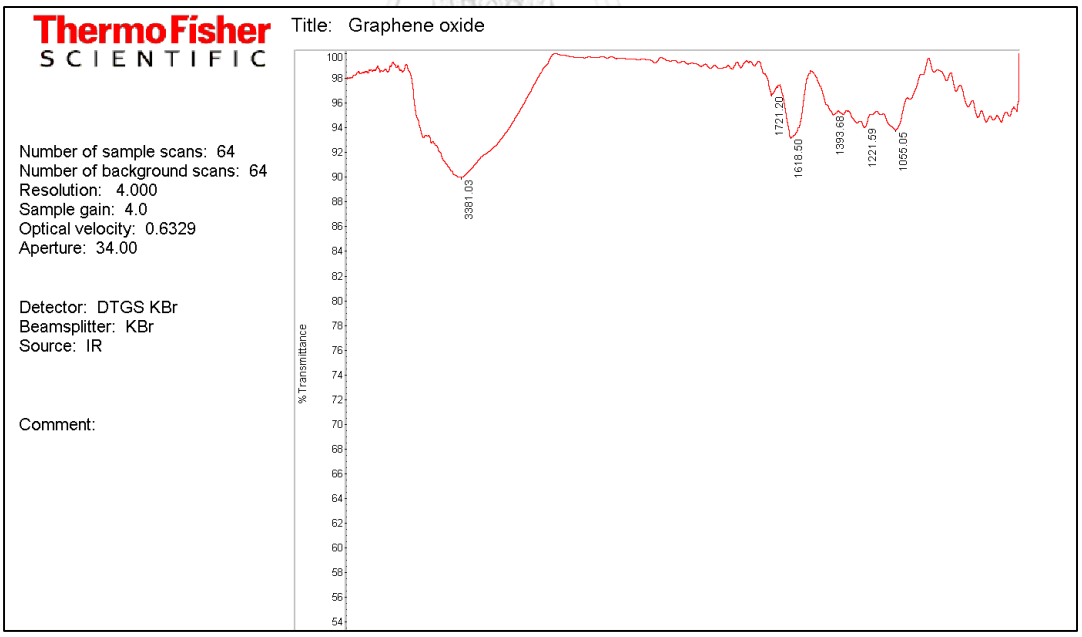

Figure a.2 FTIR spectrum of graphite oxide

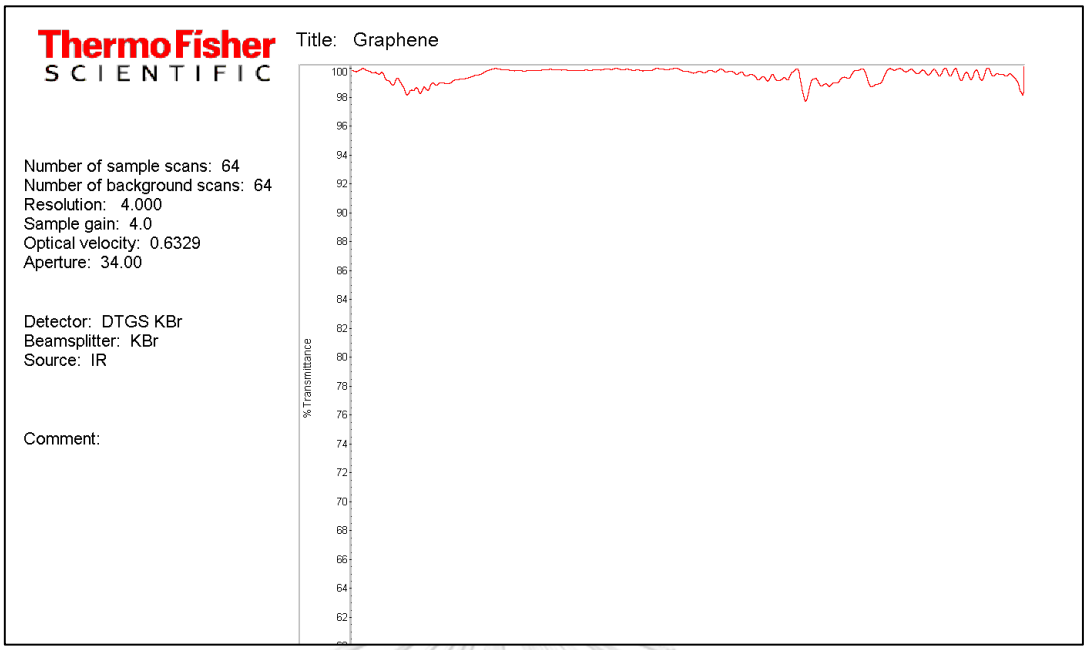

Figure a.3 FTIR spectrum of graphene

Appendix b Differential scanning calorimetry, DSC

Cooling step

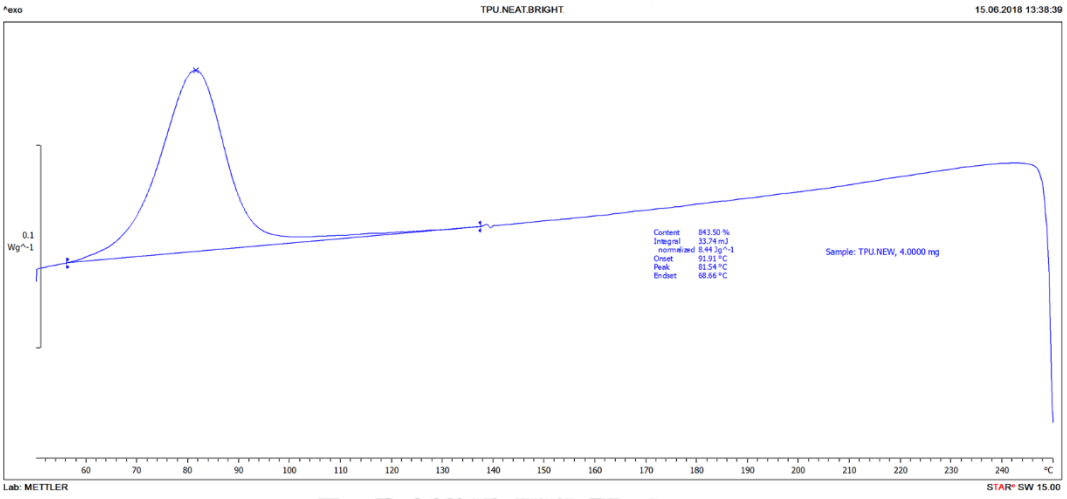

Figure b.1 DSC thermogram of TPU at cooling step.

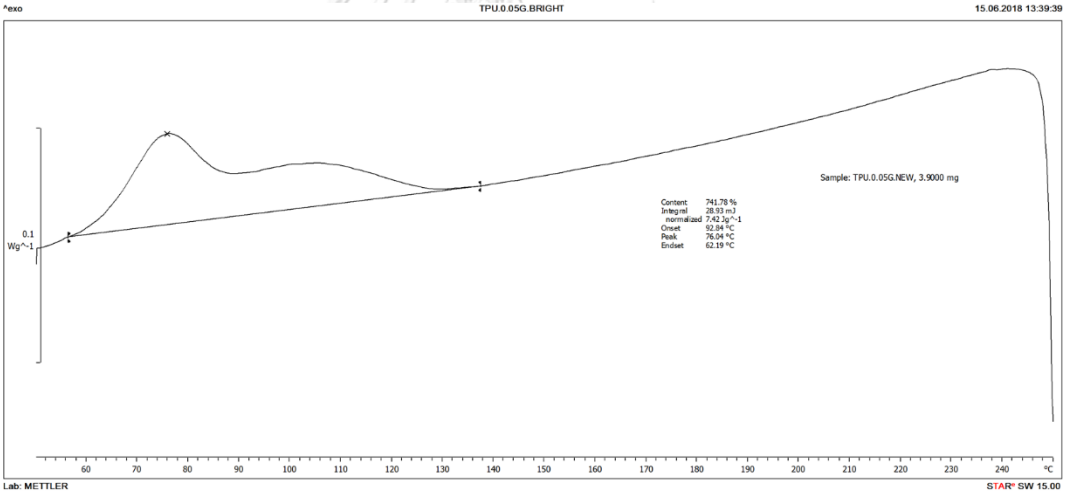

Figure b.2 DSC thermogram of TPU/0.05G at cooling step.

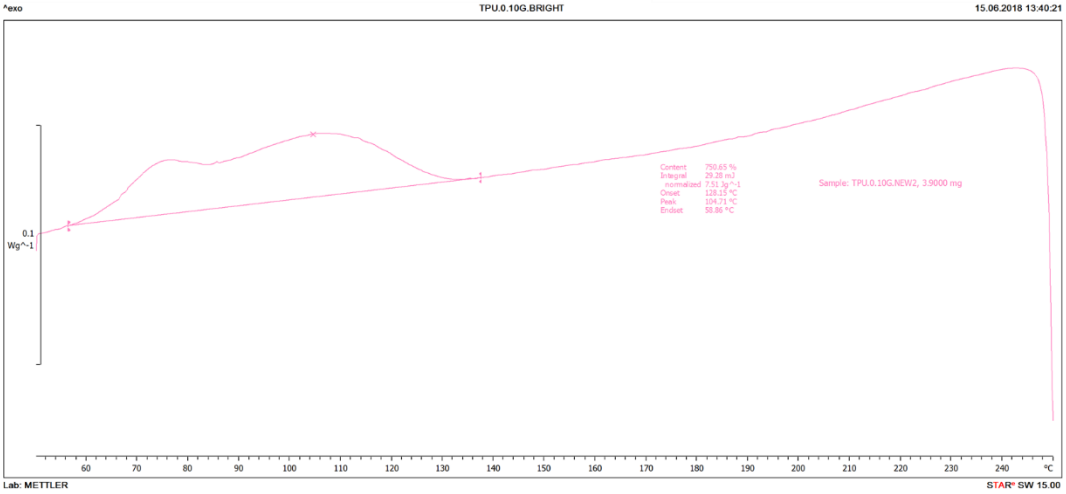

Figure b.3 DSC thermogram of TPU/0.10G at cooling step.

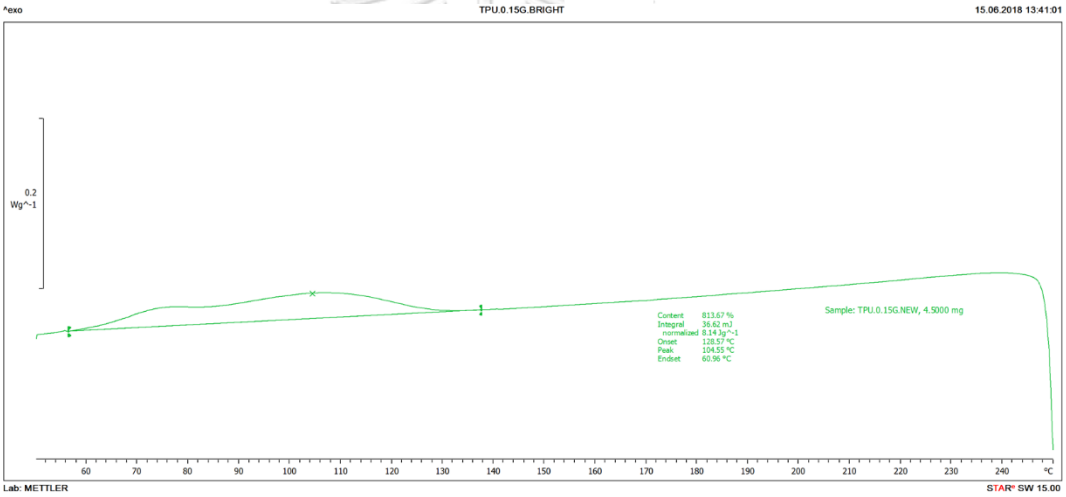

Figure b.4 DSC thermogram of TPU/0.15G at cooling step.

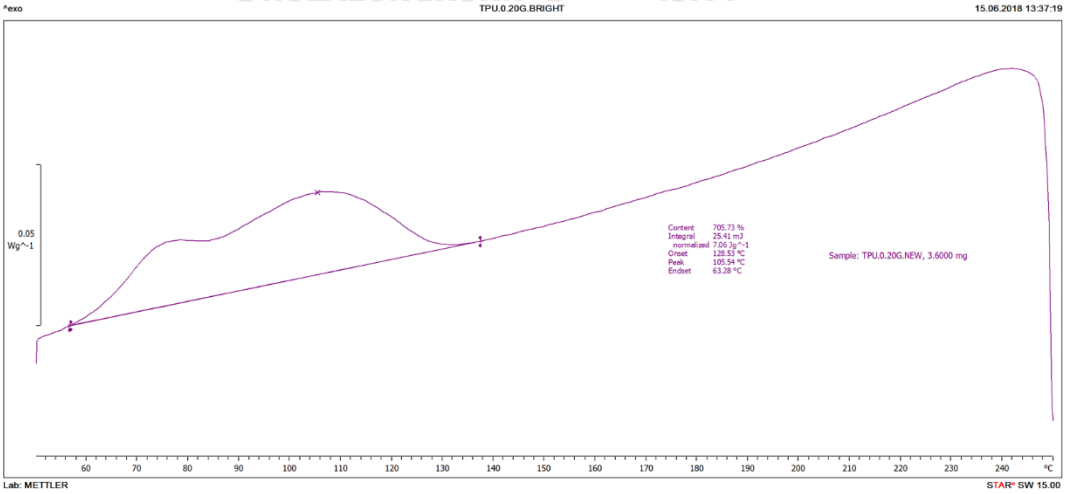

Figure b.5 DSC thermogram of TPU/0.20G at cooling step.

Heating step

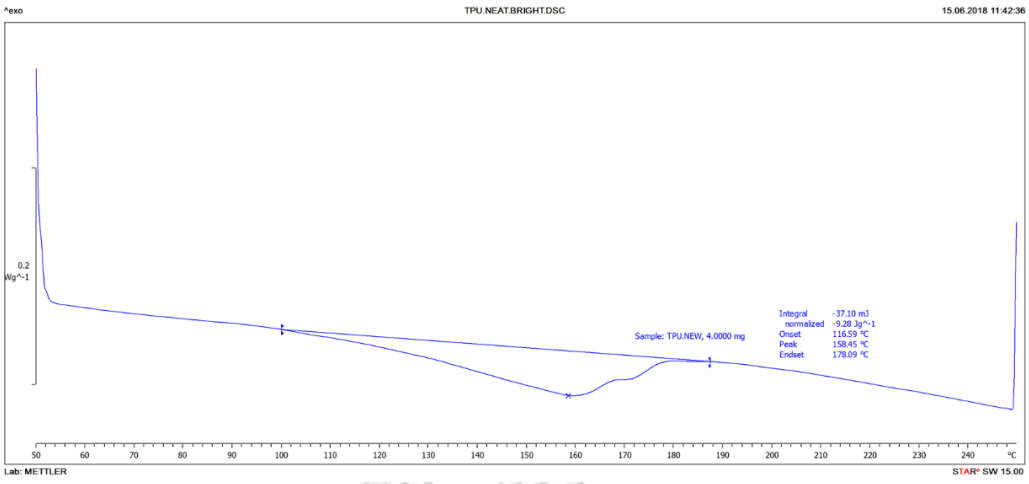

Figure b.6 DSC thermogram of TPU at second heating step.

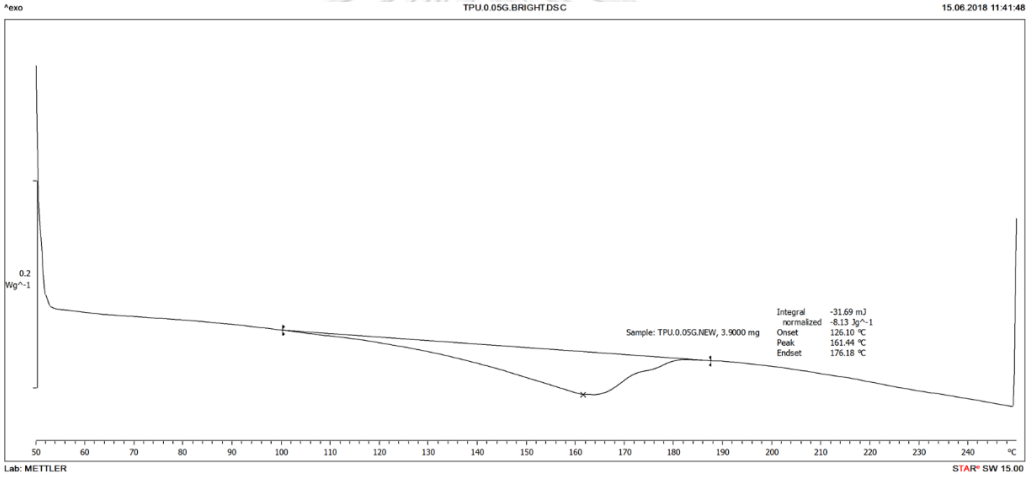

Figure b.7 DSC thermogram of TPU/0.05G at second heating step.

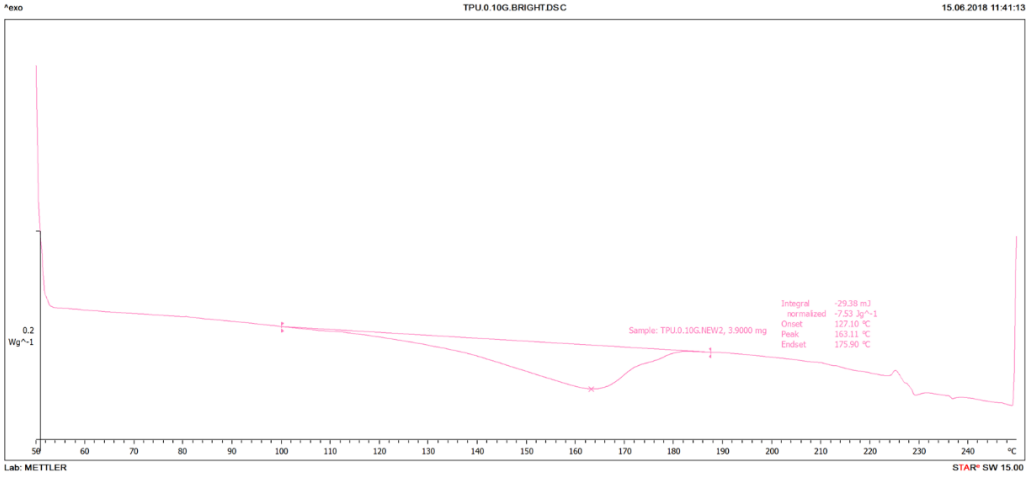

Figure b.8 DSC thermogram of TPU/0.10G at second heating step.

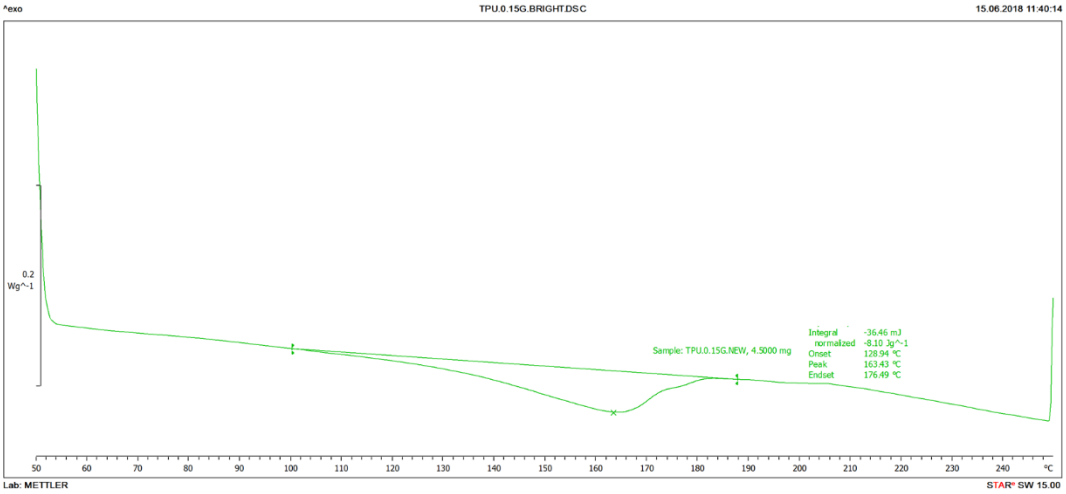

Figure b.9 DSC thermogram of TPU/0.15G at second heating step.

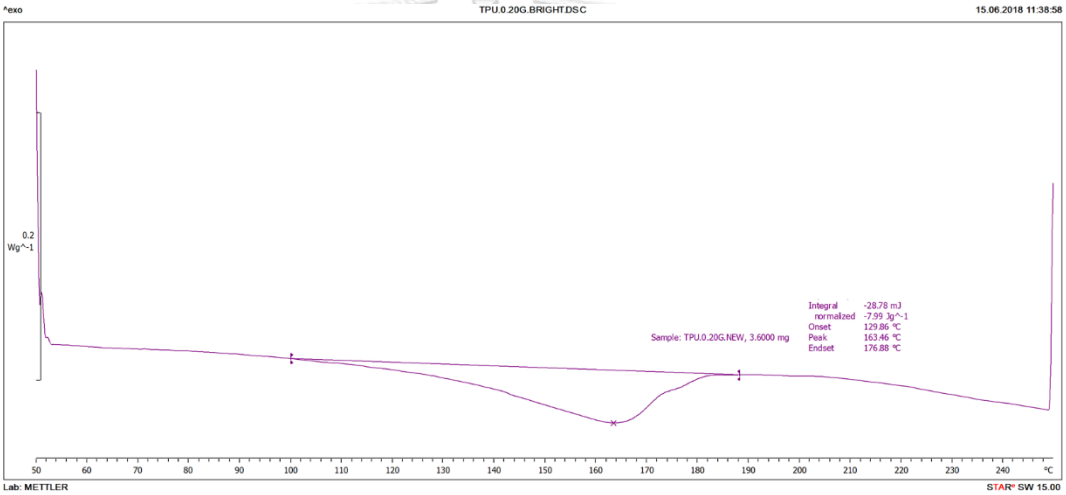

Figure b.10 DSC thermogram of TPU/0.20G at second heating step.

Appendix c Thermal gravimetric analysis, TGA

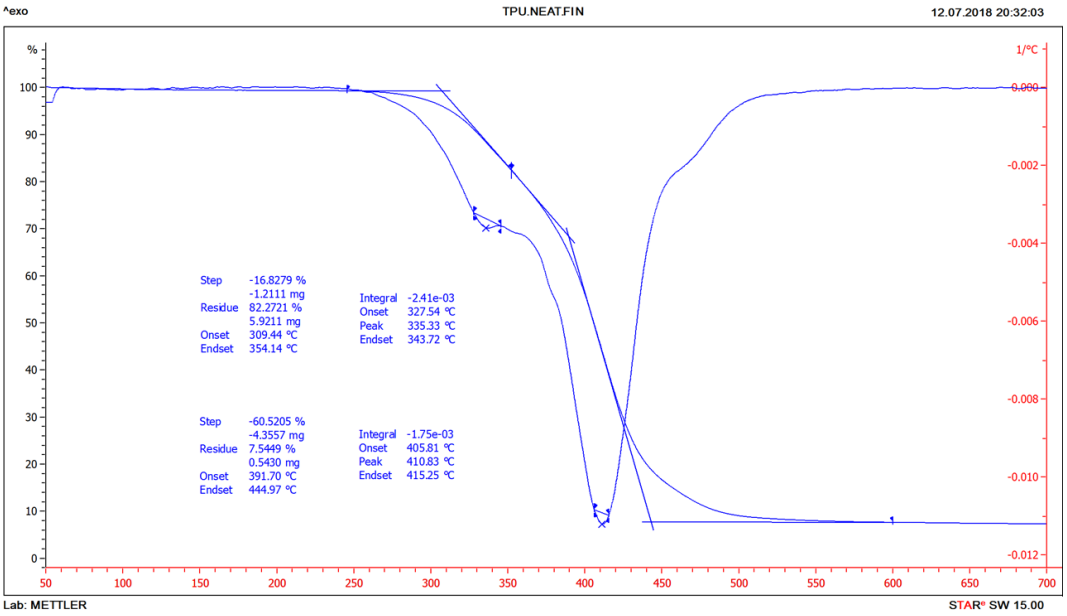

Figure c.1 TGA thermogram of TPU

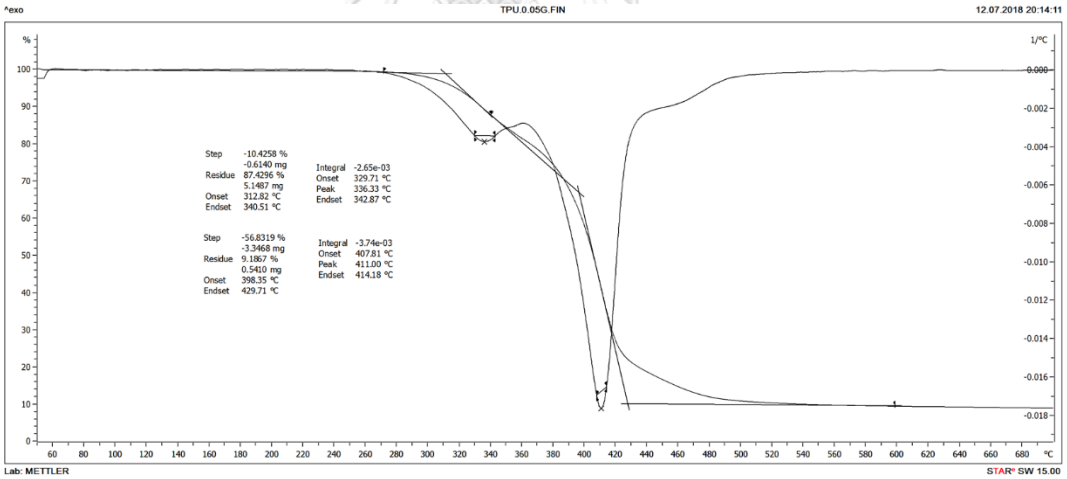

Figure c.2 TGA thermogram of TPU/0.05G

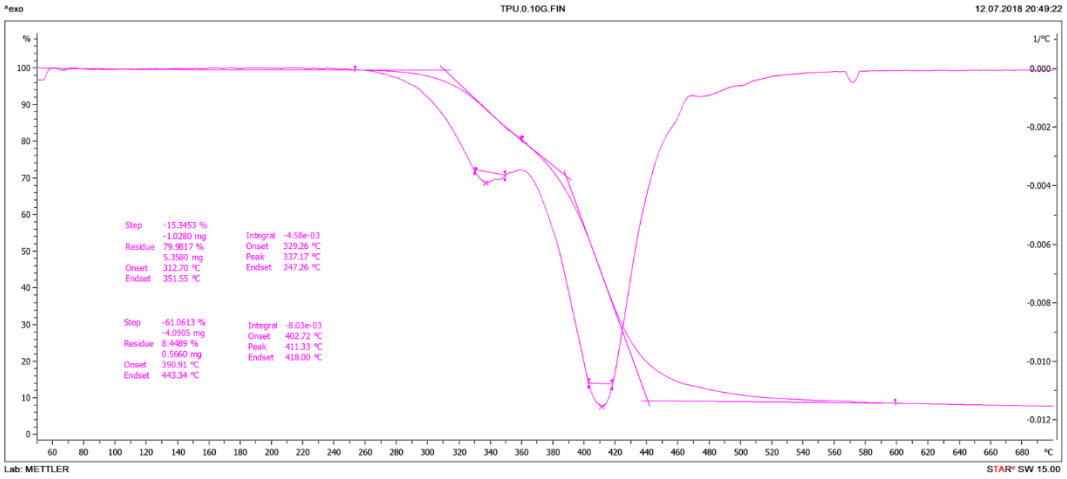

Figure c.3 TGA thermogram of TPU/0.10G

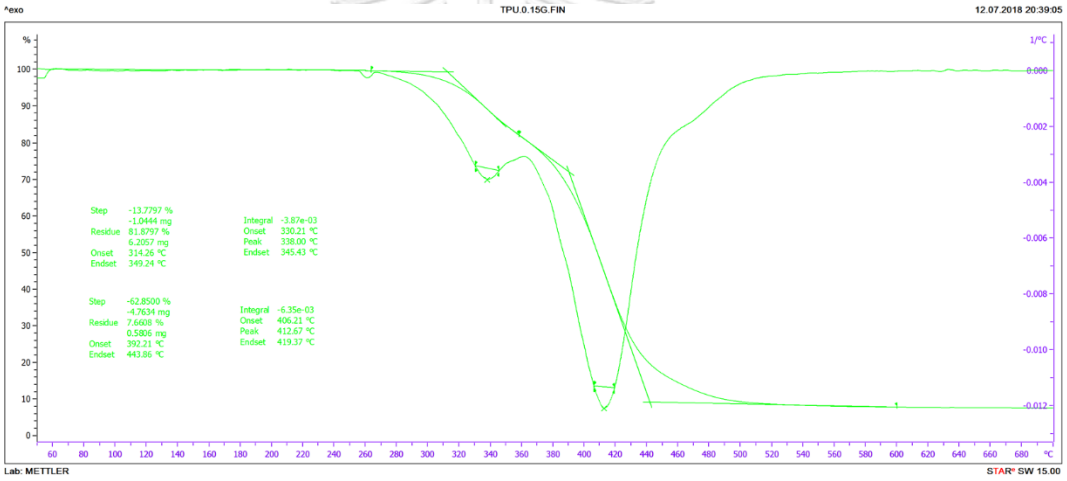

Figure c.4 TGA thermogram of TPU/0.15G

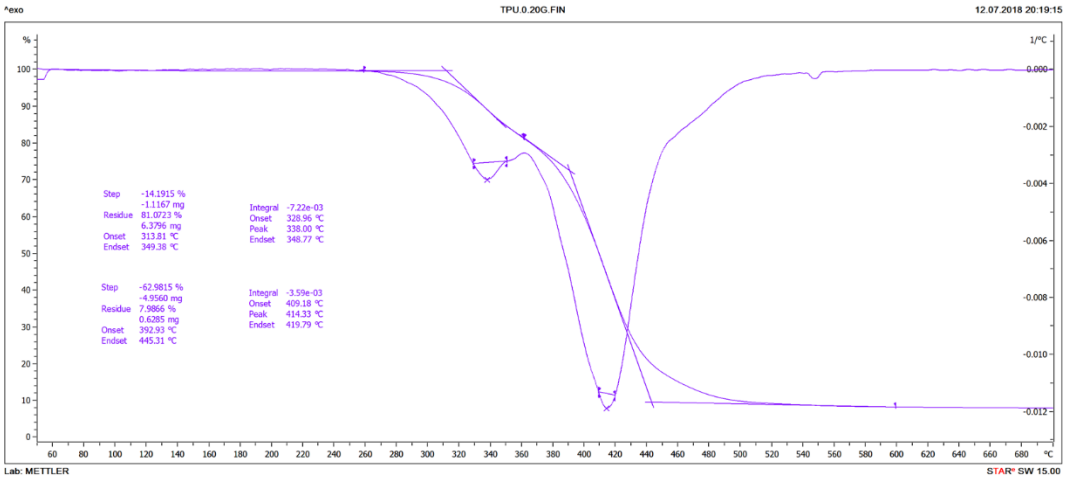

Figure c.5 TGA thermogram of TPU/0.20G

Appendix d Melt flow index

Table d.1 MFI of TPU and TPU/graphene composites

Formula	MFI (g/10min)		
	1	2	3
TPU	4.6	4.8	4.8
TPU/0.05G	3.9	4.1	4.0
TPU/0.10G	3.3	3.5	3.7
TPU/0.15G	3.5	3.3	3.4
TPU/0.20G	3.1	2.9	3.0

Statistical results

Descriptives

Melt.flow.index

	N	Mean	Std. Deviation	Std. Error	95% Confidence Interval for Mean		Minimum	Maximum
					Lower Bound	Upper Bound		
1.00	3	4.7333	.11547	.06667	4.4465	5.0202	4.60	4.80
2.00	3	4.0000	.10000	.05774	3.7516	4.2484	3.90	4.10
3.00	3	3.5000	.20000	.11547	3.0032	3.9968	3.30	3.70
4.00	3	3.4000	.10000	.05774	3.1516	3.6484	3.30	3.50
5.00	3	3.0000	.10000	.05774	2.7516	3.2484	2.90	3.10
Total	15	3.7267	.62618	.16168	3.3799	4.0734	2.90	4.80

Test of Homogeneity of Variances

Melt.flow.index

Levene Statistic	df1	df2	Sig.
.507	4	10	.732

ANOVA

Melt.flow.index

	Sum of Squares	df	Mean Square	F	Sig.
Between Groups	5.323	4	1.331	79.840	.000
Within Groups	.167	10	.017		
Total	5.489	14			

Multiple Comparisons

Dependent Variable: Melt.flow.index

LSD

(I) cat	(J) cat	Mean Difference (I-J)	Std. Error	Sig.	95% Confidence Interval	
					Lower Bound	Upper Bound
1.00	2.00	.73333*	.10541	.000	.4985	.9682
	3.00	1.23333*	.10541	.000	.9985	1.4682
	4.00	1.33333*	.10541	.000	1.0985	1.5682
	5.00	1.73333*	.10541	.000	1.4985	1.9682
2.00	1.00	-.73333*	.10541	.000	-.9682	-.4985
	3.00	.50000*	.10541	.001	.2651	.7349
	4.00	.60000*	.10541	.000	.3651	.8349
	5.00	1.00000*	.10541	.000	.7651	1.2349
3.00	1.00	-1.23333*	.10541	.000	-1.4682	-.9985
	2.00	-.50000*	.10541	.001	-.7349	-.2651
	4.00	.10000	.10541	.365	-.1349	.3349
	5.00	.50000*	.10541	.001	.2651	.7349
4.00	1.00	-1.33333*	.10541	.000	-1.5682	-1.0985
	2.00	-.60000*	.10541	.000	-.8349	-.3651
	3.00	-.10000	.10541	.365	-.3349	.1349
	5.00	.40000*	.10541	.004	.1651	.6349
5.00	1.00	-1.73333*	.10541	.000	-1.9682	-1.4985
	2.00	-1.00000*	.10541	.000	-1.2349	-.7651
	3.00	-.50000*	.10541	.001	-.7349	-.2651
	4.00	-.40000*	.10541	.004	-.6349	-.1651

*. The mean difference is significant at the 0.05 level.

Appendix e Hardness

Table e.1 Hardness of TPU and TPU/graphene composites

Formula	Hardness				
	1	2	3	4	5
TPU	72	70	71	72	69
TPU/0.05G	74	68	75	68	70
TPU/0.10G	80	78	81	70	76
TPU/0.15G	79	79	76	74	76
TPU/0.20G	72	80	79	81	76

Descriptives

Hardness

	N	Mean	Std. Deviation	Std. Error	95% Confidence Interval for Mean		Minimum	Maximum
					Lower Bound	Upper Bound		
1.00	5	70.8000	1.30384	.58310	69.1811	72.4189	69.00	72.00
2.00	5	71.0000	3.31662	1.48324	66.8819	75.1181	68.00	75.00
3.00	5	77.0000	4.35890	1.94936	71.5877	82.4123	70.00	81.00
4.00	5	76.8000	2.16795	.96954	74.1081	79.4919	74.00	79.00
5.00	5	77.6000	3.64692	1.63095	73.0718	82.1282	72.00	81.00
Total	25	74.6400	4.25127	.85025	72.8852	76.3948	68.00	81.00

Test of Homogeneity of Variances

Hardness

Levene Statistic	df1	df2	Sig.
1.775	4	20	.173

ANOVA

Hardness

	Sum of Squares	df	Mean Square	F	Sig.
Between Groups	234.960	4	58.740	5.909	.003
Within Groups	198.800	20	9.940		
Total	433.760	24			

Multiple Comparisons

Dependent Variable: Hardness

LSD

(I) cat	(J) cat	Mean Difference (I-J)	Std. Error	Sig.	95% Confidence Interval	
					Lower Bound	Upper Bound
1.00	2.00	-.20000	1.99399	.921	-4.3594	3.9594
	3.00	-6.20000*	1.99399	.006	-10.3594	-2.0406
	4.00	-6.00000*	1.99399	.007	-10.1594	-1.8406
	5.00	-6.80000*	1.99399	.003	-10.9594	-2.6406
2.00	1.00	.20000	1.99399	.921	-3.9594	4.3594
	3.00	-6.00000*	1.99399	.007	-10.1594	-1.8406
	4.00	-5.80000*	1.99399	.009	-9.9594	-1.6406
	5.00	-6.60000*	1.99399	.003	-10.7594	-2.4406
3.00	1.00	6.20000*	1.99399	.006	2.0406	10.3594
	2.00	6.00000*	1.99399	.007	1.8406	10.1594
	4.00	.20000	1.99399	.921	-3.9594	4.3594
	5.00	-.60000	1.99399	.767	-4.7594	3.5594
4.00	1.00	6.00000*	1.99399	.007	1.8406	10.1594
	2.00	5.80000*	1.99399	.009	1.6406	9.9594
	3.00	-.20000	1.99399	.921	-4.3594	3.9594
	5.00	-.80000	1.99399	.693	-4.9594	3.3594
5.00	1.00	6.80000*	1.99399	.003	2.6406	10.9594
	2.00	6.60000*	1.99399	.003	2.4406	10.7594
	3.00	.60000	1.99399	.767	-3.5594	4.7594
	4.00	.80000	1.99399	.693	-3.3594	4.9594

*. The mean difference is significant at the 0.05 level.

Appendix f Contact angle

Table f.1 Contact angle of TPU and TPU/graphene composites

Formula	Contact angle (°)				
	1	2	3	4	5
TPU	75	76	78	74	75
TPU/0.05G	76	78	80	77	77
TPU/0.10G	80	78	80	82	80
TPU/0.15G	80	80	80	81	82
TPU/0.20G	84	82	84	79	81

Descriptives

Contact.angle

	N	Mean	Std. Deviation	Std. Error	95% Confidence Interval for Mean		Minimum	Maximum
					Lower Bound	Upper Bound		
1	5	75.60	1.517	.678	73.72	77.48	74	78
2	5	77.60	1.517	.678	75.72	79.48	76	80
3	5	80.00	1.414	.632	78.24	81.76	78	82
4	5	80.60	.894	.400	79.49	81.71	80	82
5	5	82.00	2.121	.949	79.37	84.63	79	84
Total	25	79.16	2.718	.544	78.04	80.28	74	84

Test of Homogeneity of Variances

Contact.angle

Levene Statistic	df1	df2	Sig.
.731	4	20	.582

ANOVA

Contact.angle

	Sum of Squares	df	Mean Square	F	Sig.
Between Groups	129.760	4	32.440	13.630	.000
Within Groups	47.600	20	2.380		
Total	177.360	24			

Multiple Comparisons

Dependent Variable: Contact.angle

LSD

(I) cat	(J) cat	Mean Difference (I-J)	Std. Error	Sig.	95% Confidence Interval	
					Lower Bound	Upper Bound
1	2	-2.000	.976	.054	-4.04	.04
	3	-4.400*	.976	.000	-6.44	-2.36
	4	-5.000*	.976	.000	-7.04	-2.96
	5	-6.400*	.976	.000	-8.44	-4.36
2	1	2.000	.976	.054	-.04	4.04
	3	-2.400*	.976	.023	-4.44	-.36
	4	-3.000*	.976	.006	-5.04	-.96
	5	-4.400*	.976	.000	-6.44	-2.36
3	1	4.400*	.976	.000	2.36	6.44
	2	2.400*	.976	.023	.36	4.44
	4	-.600	.976	.546	-2.64	1.44
	5	-2.000	.976	.054	-4.04	.04
4	1	5.000*	.976	.000	2.96	7.04
	2	3.000*	.976	.006	.96	5.04
	3	.600	.976	.546	-1.44	2.64
	5	-1.400	.976	.167	-3.44	.64
5	1	6.400*	.976	.000	4.36	8.44
	2	4.400*	.976	.000	2.36	6.44
	3	2.000	.976	.054	-.04	4.04
	4	1.400	.976	.167	-.64	3.44

*. The mean difference is significant at the 0.05 level.

Appendix g Tensile properties

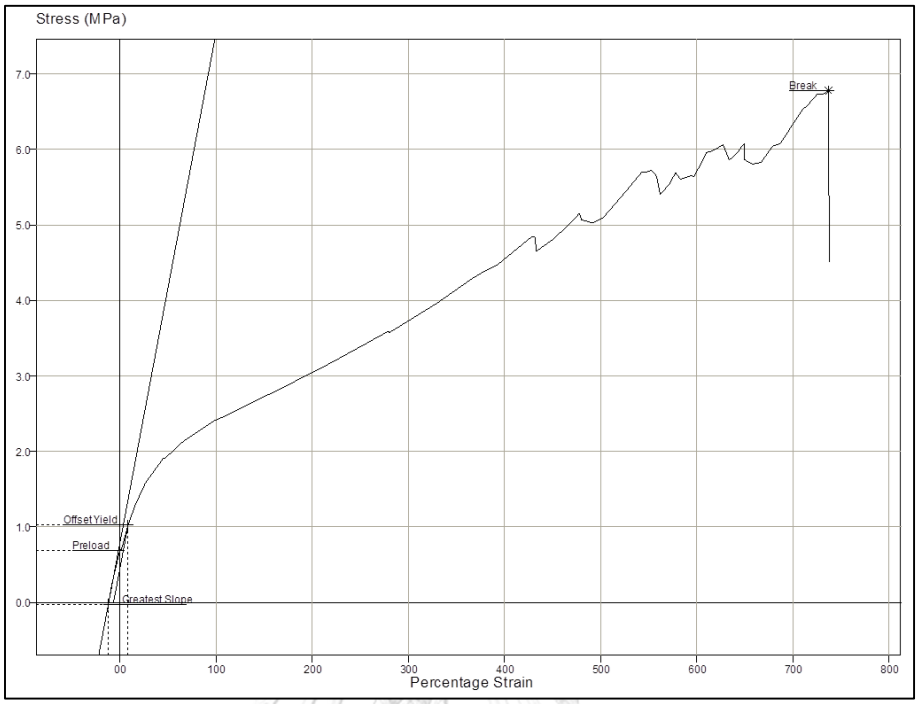

Figure g.1 Tensile result of TPU (test 1)

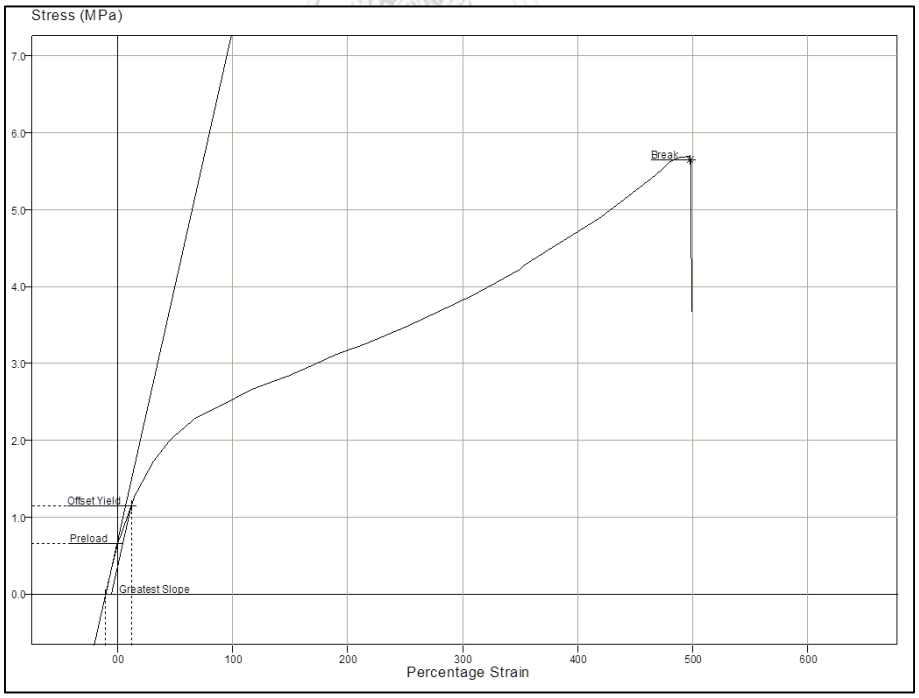

Figure g.2 Tensile result of TPU/0.05G (test 1)

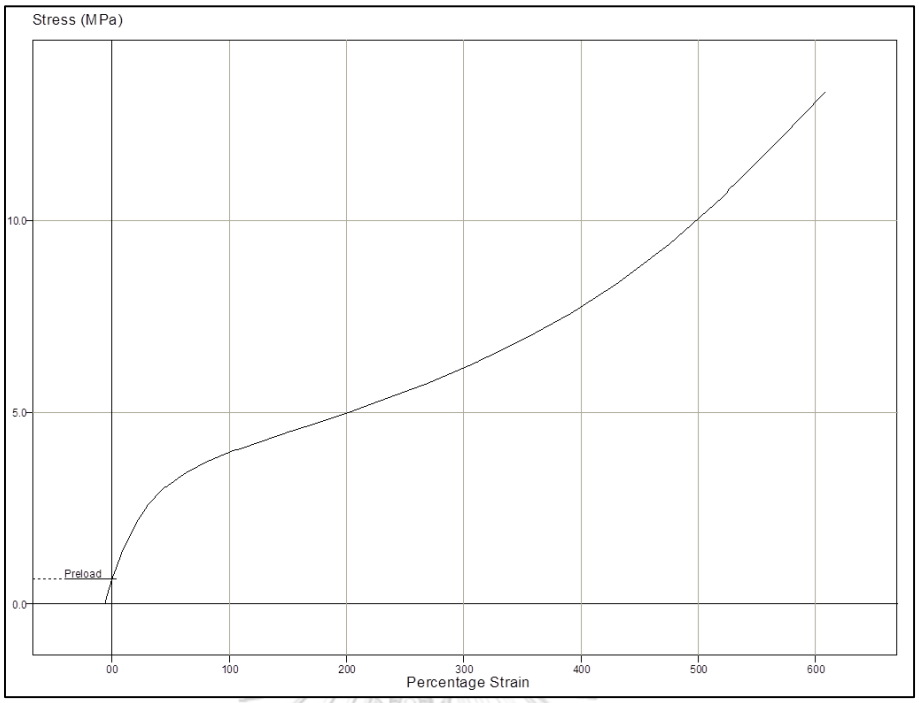

Figure g.3 Tensile result of TPU/0.05G (test 2)

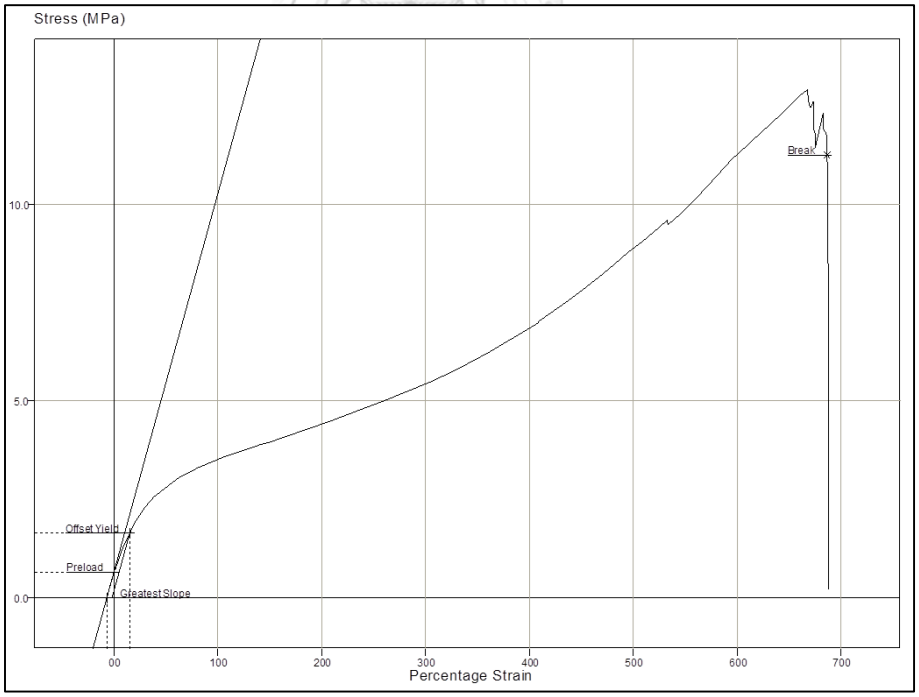

Figure g.4 Tensile result of TPU/0.05G (test 3)

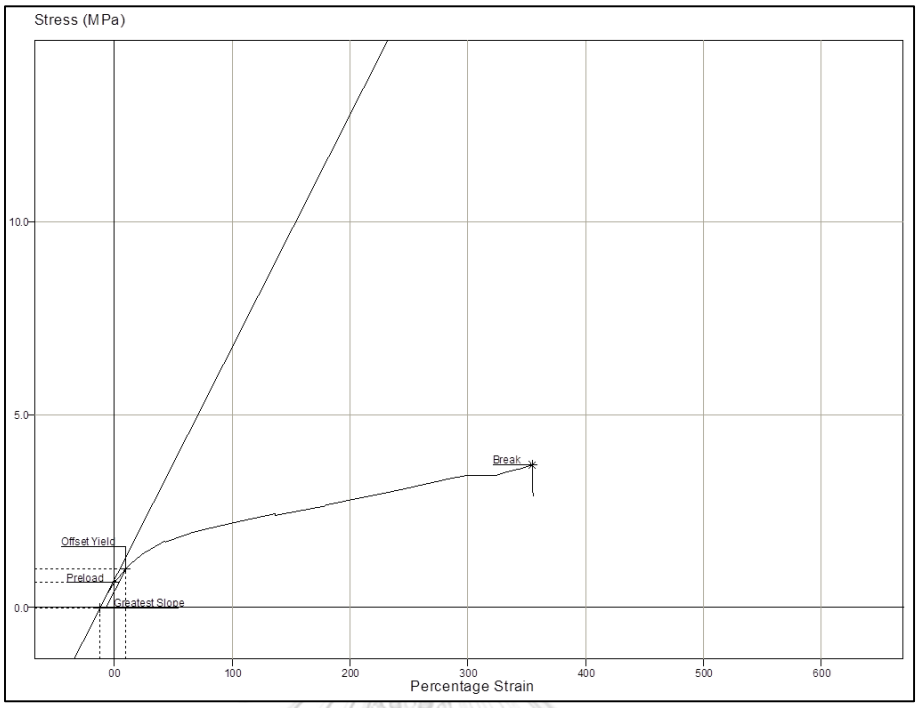

Figure g.5 Tensile result of TPU/0.10G (test 1)

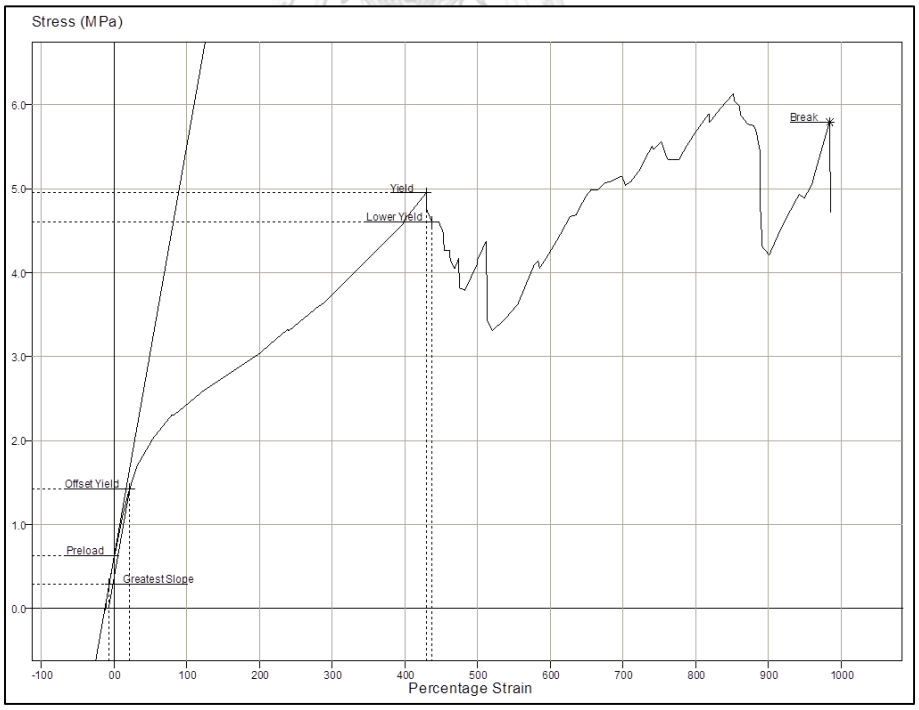

Figure g.6 Tensile result of TPU/0.10G (test 2)

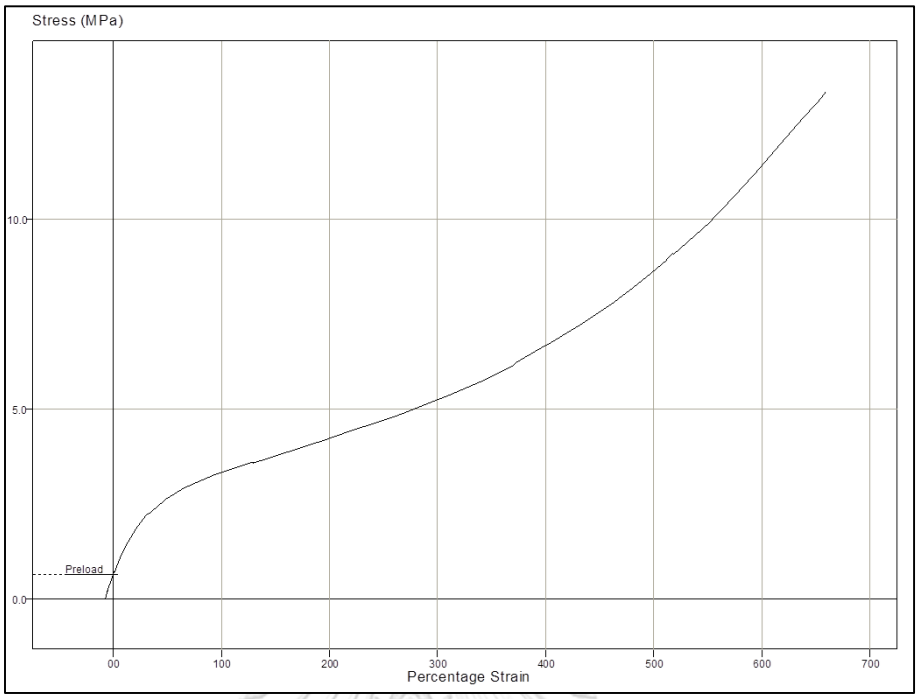

Figure g.7 Tensile result of TPU/0.10G (test 3)

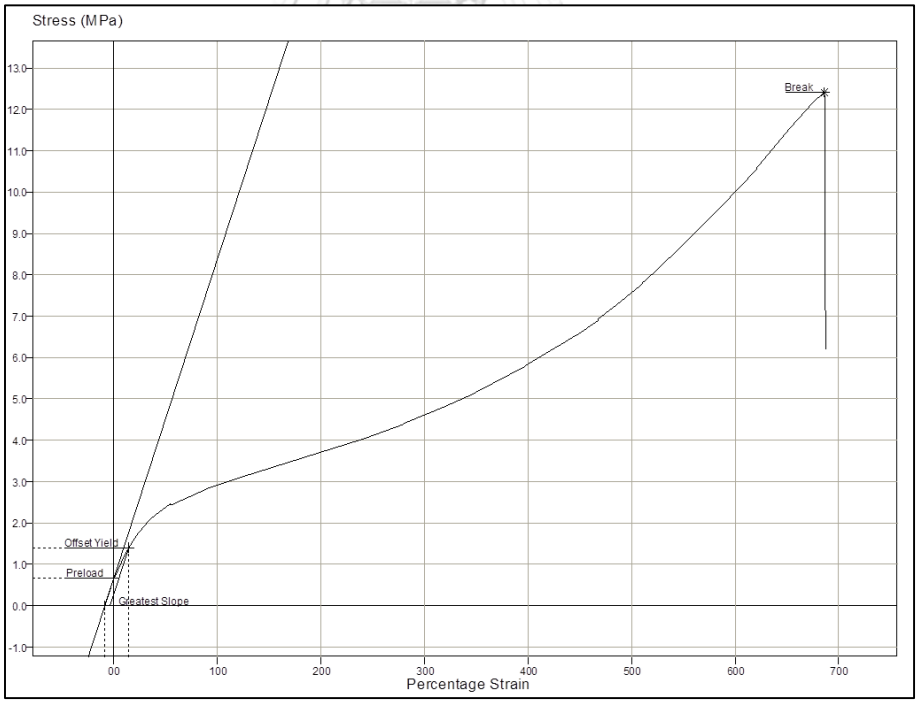

Figure g.8 Tensile result of TPU/0.15G (test 1)

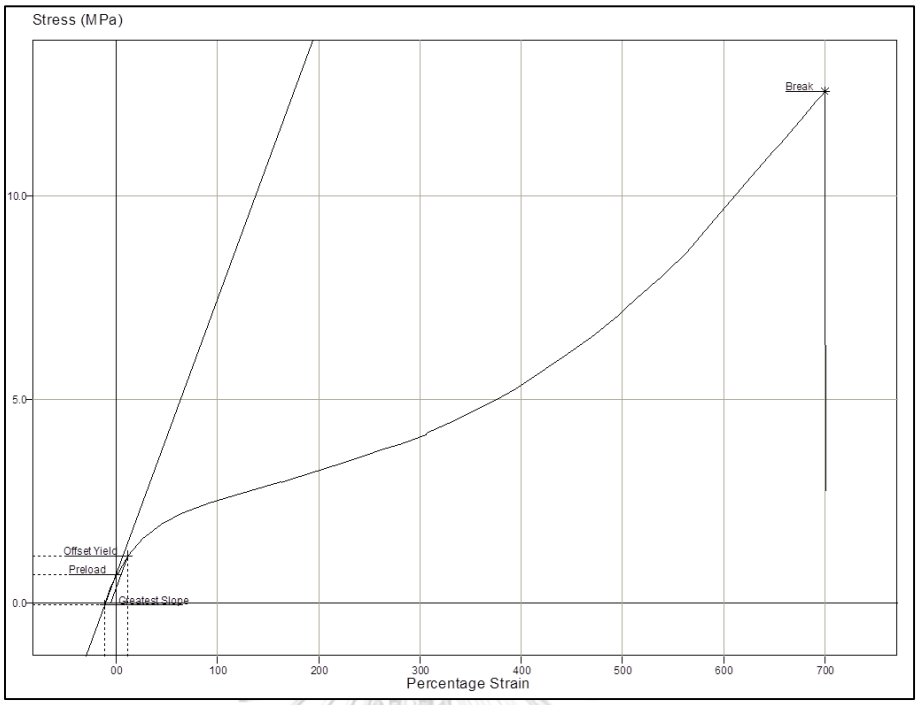

Figure g.9 Tensile result of TPU/0.15G (test 2)

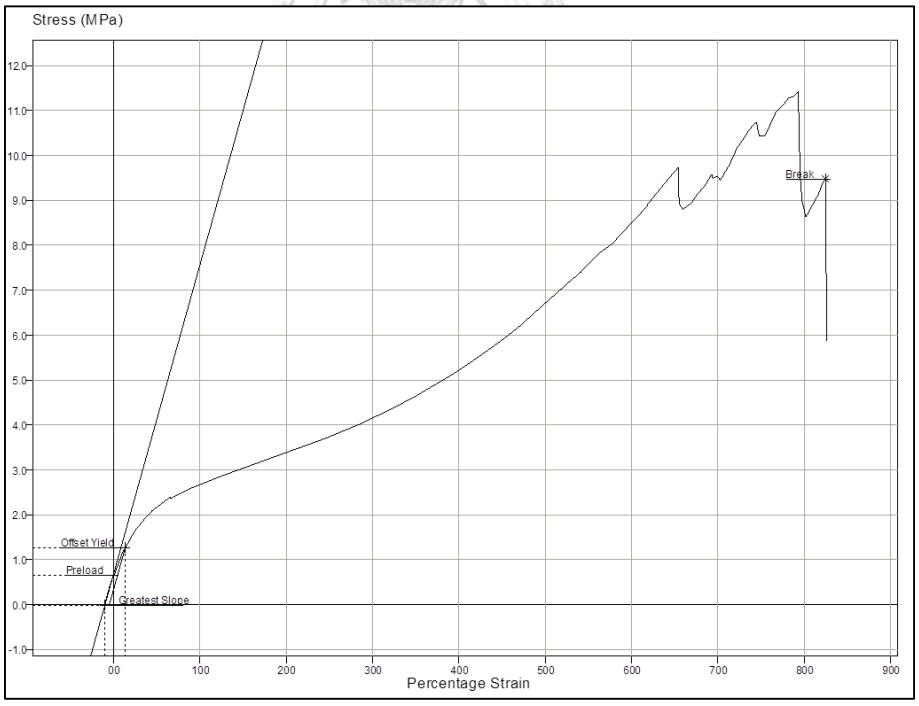

Figure g.10 Tensile result of TPU/0.15G (test 3)

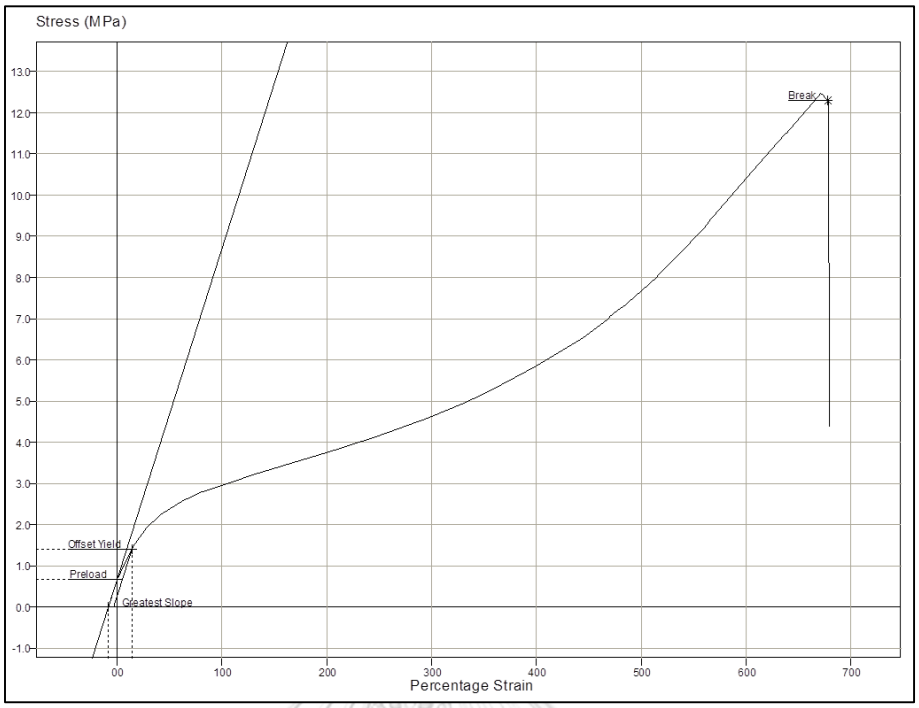

Figure g.11 Tensile result of TPU/0.20G (test 1)

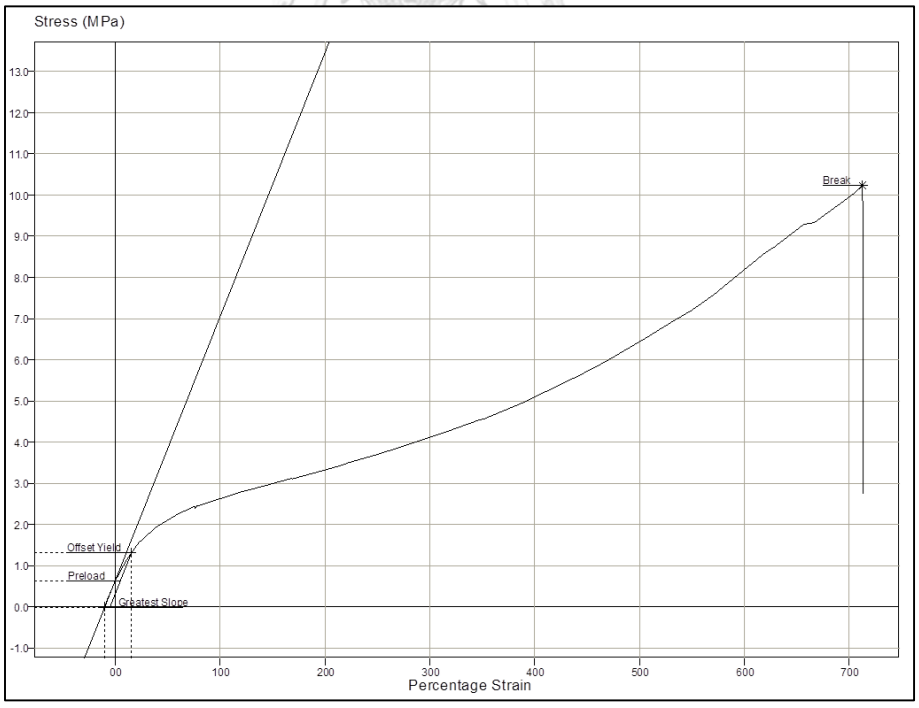

Figure g.12 Tensile result of TPU/0.20G (test 2)

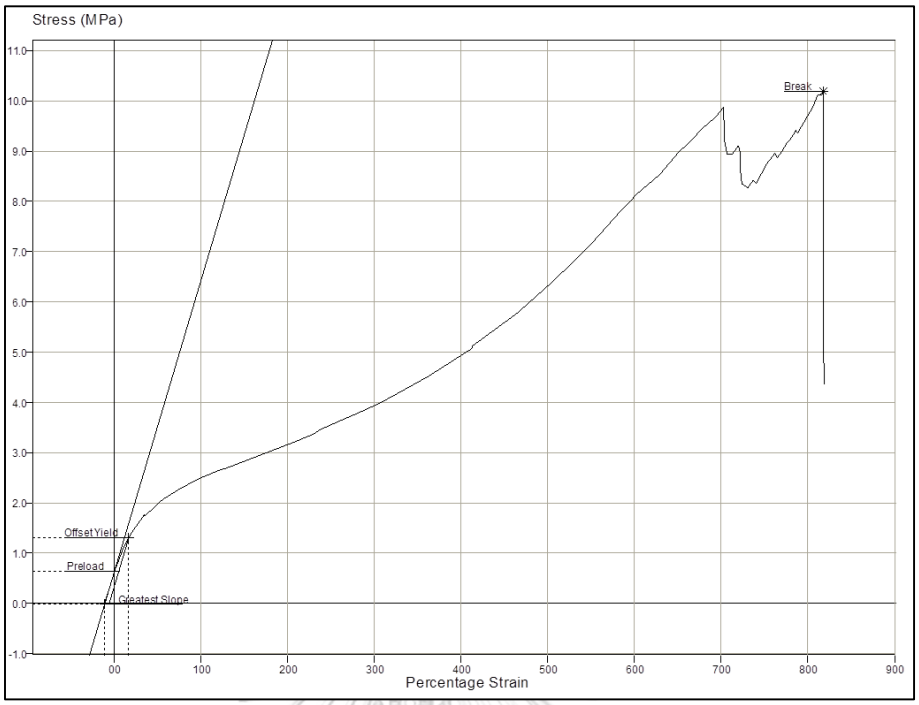

Figure g.13 Tensile result of TPU/0.20G (test 3)

Table g.1 Young's modulus of TPU and TPU/graphene composites

Formula	Young's modulus (MPa)		
	1	2	3
TPU	6.75	-	-
TPU/0.05G	6.65	12.97	9.61
TPU/0.10G	6.02	4.89	8.42
TPU/0.15G	7.71	6.75	6.88
TPU/0.20G	8.03	6.41	5.80

Descriptives

Tensile.modulus

	N	Mean	Std. Deviation	Std. Error	95% Confidence Interval for Mean		Minimum	Maximum
					Lower Bound	Upper Bound		
1.00	3	6.7543	.00000	.00000	6.7543	6.7543	6.75	6.75
2.00	3	9.7458	3.16454	1.82705	1.8847	17.6070	6.65	12.97
3.00	3	6.4470	1.80440	1.04177	1.9646	10.9293	4.89	8.42
4.00	3	7.1141	.52194	.30134	5.8176	8.4107	6.75	7.71
5.00	3	6.7463	1.15487	.66677	3.8774	9.6151	5.80	8.03
Total	15	7.3615	1.92246	.49638	6.2969	8.4261	4.89	12.97

Test of Homogeneity of Variances

Tensile.modulus

Levene Statistic	df1	df2	Sig.
2.634	4	10	.098

ANOVA

Tensile.modulus

	Sum of Squares	df	Mean Square	F	Sig.
Between Groups	21.990	4	5.497	1.848	.196
Within Groups	29.753	10	2.975		
Total	51.742	14			

Multiple Comparisons

Dependent Variable: Tensile.modulus

LSD

(I) Cat	(J) Cat	Mean Difference (I-J)	Std. Error	Sig.	95% Confidence Interval	
					Lower Bound	Upper Bound
1.00	2.00	-2.99157	1.40837	.060	-6.1296	.1465
	3.00	.30730	1.40837	.832	-2.8307	3.4453
	4.00	-.35987	1.40837	.803	-3.4979	2.7782
	5.00	.00798	1.40837	.996	-3.1301	3.1460
2.00	1.00	2.99157	1.40837	.060	-.1465	6.1296
	3.00	3.29887*	1.40837	.041	.1608	6.4369
	4.00	2.63170	1.40837	.091	-.5063	5.7697
	5.00	2.99956	1.40837	.059	-.1385	6.1376
3.00	1.00	-.30730	1.40837	.832	-3.4453	2.8307
	2.00	-3.29887*	1.40837	.041	-6.4369	-.1608
	4.00	-.66717	1.40837	.646	-3.8052	2.4709
	5.00	-.29931	1.40837	.836	-3.4374	2.8387
4.00	1.00	.35987	1.40837	.803	-2.7782	3.4979
	2.00	-2.63170	1.40837	.091	-5.7697	.5063
	3.00	.66717	1.40837	.646	-2.4709	3.8052
	5.00	.36786	1.40837	.799	-2.7702	3.5059
5.00	1.00	-.00798	1.40837	.996	-3.1460	3.1301
	2.00	-2.99956	1.40837	.059	-6.1376	.1385
	3.00	.29931	1.40837	.836	-2.8387	3.4374
	4.00	-.36786	1.40837	.799	-3.5059	2.7702

*. The mean difference is significant at the 0.05 level.

Table ง.2 Stress at 100 mm strain of TPU and TPU/graphene composites

Formula	Stress at 100 mm (MPa)		
	1	2	3
TPU	3.66	-	-
TPU/0.05G	3.85	6.11	5.39
TPU/0.10G	3.38	3.65	5.19
TPU/0.15G	4.55	3.99	4.09
TPU/0.20G	4.57	4.06	3.87

Descriptives

Tensile.stress@100mm

	N	Mean	Std. Deviation	Std. Error	95% Confidence Interval for Mean		Minimum	Maximum
					Lower Bound	Upper Bound		
1.00	3	3.6587	.00000	.00000	3.6587	3.6587	3.66	3.66
2.00	3	5.1205	1.15600	.66742	2.2488	7.9922	3.85	6.11
3.00	3	4.0742	.97906	.56526	1.6421	6.5063	3.38	5.19
4.00	3	4.2112	.30042	.17345	3.4649	4.9575	3.99	4.55
5.00	3	4.1672	.36244	.20926	3.2669	5.0676	3.87	4.57
Total	15	4.2464	.77795	.20087	3.8156	4.6772	3.38	6.11

Test of Homogeneity of Variances

Tensile.stress@100mm

Levene Statistic	df1	df2	Sig.
4.651	4	10	.022

ANOVA

Tensile.stress@100mm

	Sum of Squares	df	Mean Square	F	Sig.
Between Groups	3.440	4	.860	1.709	.224
Within Groups	5.033	10	.503		
Total	8.473	14			

Multiple Comparisons

Dependent Variable: Tensile.stress@100mm

LSD

(I) Cat	(J) Cat	Mean Difference (I-J)	Std. Error	Sig.	95% Confidence Interval	
					Lower Bound	Upper Bound
1.00	2.00	-1.46183*	.57925	.030	-2.7525	-.1712
	3.00	-.41554	.57925	.490	-1.7062	.8751
	4.00	-.55253	.57925	.363	-1.8432	.7381
	5.00	-.50856	.57925	.401	-1.7992	.7821
2.00	1.00	1.46183*	.57925	.030	.1712	2.7525
	3.00	1.04628	.57925	.101	-.2444	2.3369
	4.00	.90930	.57925	.148	-.3814	2.2000
	5.00	.95327	.57925	.131	-.3374	2.2439
3.00	1.00	.41554	.57925	.490	-.8751	1.7062
	2.00	-1.04628	.57925	.101	-2.3369	.2444
	4.00	-.13698	.57925	.818	-1.4276	1.1537
	5.00	-.09301	.57925	.876	-1.3837	1.1976
4.00	1.00	.55253	.57925	.363	-.7381	1.8432
	2.00	-.90930	.57925	.148	-2.2000	.3814
	3.00	.13698	.57925	.818	-1.1537	1.4276
	5.00	.04397	.57925	.941	-1.2467	1.3346
5.00	1.00	.50856	.57925	.401	-.7821	1.7992
	2.00	-.95327	.57925	.131	-2.2439	.3374
	3.00	.09301	.57925	.876	-1.1976	1.3837
	4.00	-.04397	.57925	.941	-1.3346	1.2467

*. The mean difference is significant at the 0.05 level.

Appendix h Electrical conductivity

Table h.1 Resistance of TPU and TPU/graphene composites

Order	Resistance (TΩ)				
	TPU	TPU/0.05G	TPU/0.10G	TPU/0.15G	TPU/0.20G
1	1.57	0.58	0.34	0.60	0.24
2	1.26	0.58	0.44	0.57	0.49
3	0.73	1.03	0.87	0.49	0.23
4	0.56	0.61	0.30	0.80	0.38
5	1.16	0.76	0.45	0.59	0.29
6	0.98	0.68	0.88	0.38	0.37
7	0.76	0.77	0.60	0.41	0.28
8	0.58	1.48	0.81	0.30	0.24
9	0.73	0.60	0.37	0.32	0.44
10	0.73	0.49	0.68	0.49	0.57

Descriptives

Resistance

	N	Mean	Std. Deviation	Std. Error	95% Confidence Interval for Mean		Minimum	Maximum
					Lower Bound	Upper Bound		
1.00	10	.9060	.32938	.10416	.6704	1.1416	.56	1.57
2.00	10	.7580	.29506	.09331	.5469	.9691	.49	1.48
3.00	10	.5750	.22477	.07108	.4142	.7358	.30	.88
4.00	10	.4950	.15197	.04806	.3863	.6037	.30	.80
5.00	10	.3530	.11757	.03718	.2689	.4371	.23	.57
Total	50	.6174	.30117	.04259	.5318	.7030	.23	1.57

Test of Homogeneity of Variances

Resistance

Levene Statistic	df1	df2	Sig.
2.708	4	45	.042

ANOVA

Resistance

	Sum of Squares	df	Mean Square	F	Sig.
Between Groups	1.897	4	.474	8.381	.000
Within Groups	2.547	45	.057		
Total	4.444	49			

Multiple Comparisons

Dependent Variable: Resistance

LSD

(I) cat	(J) cat	Mean Difference (I-J)	Std. Error	Sig.	95% Confidence Interval	
					Lower Bound	Upper Bound
1.00	2.00	.14800	.10639	.171	-.0663	.3623
	3.00	.33103*	.10639	.003	.1167	.5453
	4.00	.41100*	.10639	.000	.1967	.6253
	5.00	.55300*	.10639	.000	.3387	.7673
2.00	1.00	-.14800	.10639	.171	-.3623	.0663
	3.00	.18303	.10639	.092	-.0313	.3973
	4.00	.26300*	.10639	.017	.0487	.4773
	5.00	.40500*	.10639	.000	.1907	.6193
3.00	1.00	-.33103*	.10639	.003	-.5453	-.1167
	2.00	-.18303	.10639	.092	-.3973	.0313
	4.00	.07997	.10639	.456	-.1343	.2943
	5.00	.22197*	.10639	.043	.0077	.4363
4.00	1.00	-.41100*	.10639	.000	-.6253	-.1967
	2.00	-.26300*	.10639	.017	-.4773	-.0487
	3.00	-.07997	.10639	.456	-.2943	.1343
	5.00	.14200	.10639	.189	-.0723	.3563
5.00	1.00	-.55300*	.10639	.000	-.7673	-.3387
	2.00	-.40500*	.10639	.000	-.6193	-.1907
	3.00	-.22197*	.10639	.043	-.4363	-.0077
	4.00	-.14200	.10639	.189	-.3563	.0723

*. The mean difference is significant at the 0.05 level.

Table h.2 Conductivity of TPU and TPU/graphene composites

Order	Conductivity (nS/m)				
	TPU	TPU/0.05G	TPU/0.10G	TPU/0.15G	TPU/0.20G
1	2.42	7.25	12.48	6.97	18.18
2	3.03	7.17	9.55	7.43	8.78
3	5.20	4.05	4.87	8.63	19.29
4	6.78	6.85	14.33	5.28	11.43
5	3.30	5.52	9.38	7.09	15.05
6	3.90	6.18	4.82	10.96	11.77
7	4.98	5.46	7.02	10.24	15.27
8	6.54	2.82	5.24	13.99	18.17
9	5.25	7.00	11.39	12.98	9.85
10	5.22	8.45	6.26	8.61	7.58

Descriptives

Conductivity

	N	Mean	Std. Deviation	Std. Error	95% Confidence Interval for Mean		Minimum	Maximum
					Lower Bound	Upper Bound		
1.00	10	4.6500	1.46230	.46242	3.6039	5.6961	2.40	6.80
2.00	10	6.0700	1.68328	.53230	4.8659	7.2741	2.80	8.50
3.00	10	8.5400	3.41051	1.07850	6.1003	10.9797	4.80	14.30
4.00	10	9.2200	2.79157	.88277	7.2230	11.2170	5.30	14.00
5.00	10	13.5500	4.22223	1.33519	10.5296	16.5704	7.60	19.30
Total	50	8.4060	4.15778	.58800	7.2244	9.5876	2.40	19.30

Test of Homogeneity of Variances

Conductivity

Levene Statistic	df1	df2	Sig.
6.162	4	45	.000

ANOVA

Conductivity

	Sum of Squares	df	Mean Square	F	Sig.
Between Groups	467.057	4	116.764	13.827	.000
Within Groups	380.011	45	8.445		
Total	847.068	49			

Multiple Comparisons

Dependent Variable: Conductivity

LSD

(I) cat	(J) cat	Mean Difference (I-J)	Std. Error	Sig.	95% Confidence Interval	
					Lower Bound	Upper Bound
1.00	2.00	-1.42000	1.29959	.280	-4.0375	1.1975
	3.00	-3.89000*	1.29959	.004	-6.5075	-1.2725
	4.00	-4.57000*	1.29959	.001	-7.1875	-1.9525
	5.00	-8.90000*	1.29959	.000	-11.5175	-6.2825
2.00	1.00	1.42000	1.29959	.280	-1.1975	4.0375
	3.00	-2.47000	1.29959	.064	-5.0875	.1475
	4.00	-3.15000*	1.29959	.019	-5.7675	-.5325
	5.00	-7.48000*	1.29959	.000	-10.0975	-4.8625
3.00	1.00	3.89000*	1.29959	.004	1.2725	6.5075
	2.00	2.47000	1.29959	.064	-.1475	5.0875
	4.00	-.68000	1.29959	.603	-3.2975	1.9375
	5.00	-5.01000*	1.29959	.000	-7.6275	-2.3925
4.00	1.00	4.57000*	1.29959	.001	1.9525	7.1875
	2.00	3.15000*	1.29959	.019	.5325	5.7675
	3.00	.68000	1.29959	.603	-1.9375	3.2975
	5.00	-4.33000*	1.29959	.002	-6.9475	-1.7125
5.00	1.00	8.90000*	1.29959	.000	6.2825	11.5175
	2.00	7.48000*	1.29959	.000	4.8625	10.0975
	3.00	5.01000*	1.29959	.000	2.3925	7.6275
	4.00	4.33000*	1.29959	.002	1.7125	6.9475

*. The mean difference is significant at the 0.05 level.

VITA

Mr. Warrayut Kanabenja was born on May 17, 1994 in Bangkok, Thailand. He graduated the Bachelor Degree of Engineering in Petrochemical and Polymeric Materials from Faculty of Engineering and Industrial technology, Silpakorn University in 2015. For a one year later, he continually study in Master Degree of Applied Polymer Science and Textile Technology at Department of Materials Science, Faculty of Science, Chulalongkorn University and finally graduated his Master's Degree on August 2018.

International Presentation:

1. W. Kanabenja and P. Potiyaraj, "Graphene/thermoplastic polyurethane composites", The Third International Conference on Applied Engineering, Materials and Mechanics, Okinawa Island, Japan, April 20-22, 2018.